CRREL REPORT 95-24

Ground-Penetrating Radar Investigation of the Proposed Dome–CARA Tunnel Route and Utilities at South Pole Station, Antarctica

Steven A. Arcone, Wayne Tobiasson
and Allan J. Delaney

December 1995

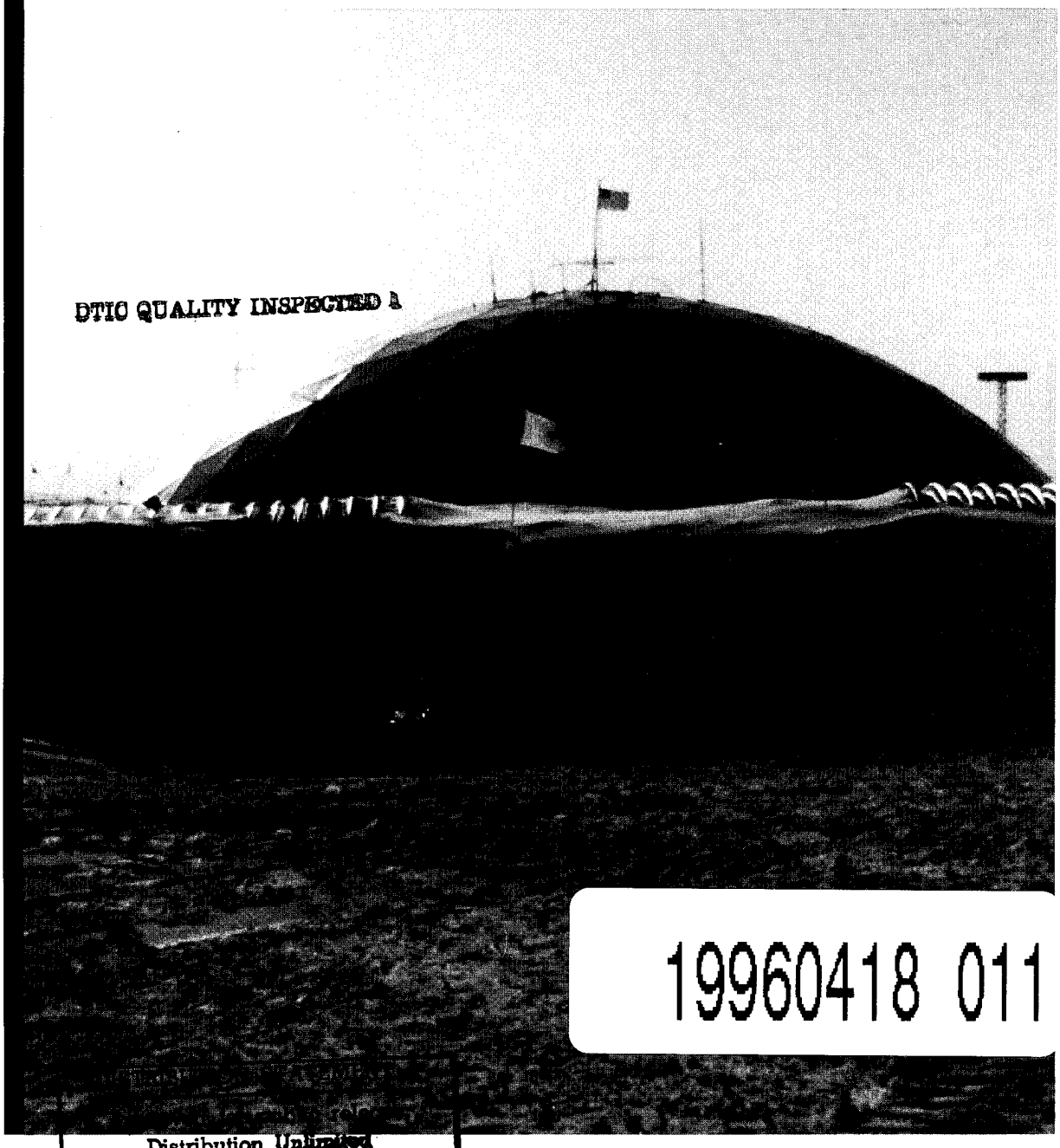

DISCLAIMER NOTICE

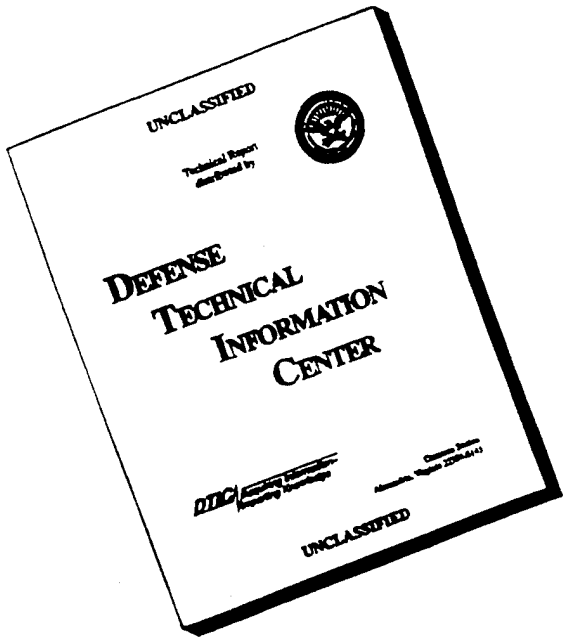

THIS DOCUMENT IS BEST QUALITY AVAILABLE. THE COPY FURNISHED TO DTIC CONTAINED A SIGNIFICANT NUMBER OF PAGES WHICH DO NOT REPRODUCE LEGIBLY.

Abstract

Ground-penetrating radar studies were performed at South Pole Station, Antarctica, during January 1993 to determine if subsurface obstructions exist along a planned tunnel route from the main station to the new astrophysical research area on the far side of the skiway, and if various man-made subsurface features such as sewage sumps, a water well, utilidors and buried buildings could be located and delineated. The maximum depth of interest for the tunnel survey was approximately 10 m. For it, a short-pulse antenna transducer with its antenna bandwidth centered near 400 MHz was towed along the ground surface over multiple traverses to cover an area up to 60 m wide. The survey extended from the South Pole Station fuel arch, across the skiway and then to the CARA site (Center for Astrophysical Research in Antarctica). The radar profiles show reflections from density layering within the snow caused by traffic and diffractions from artificial features within 13 m depth. Debris is present in the snow west of the skiway and near the fuel bladder near the taxiway. Targets within 100 m of the west side of the skiway are extensive, and appear to be metallic. The tunnel should be routed in the clear area north of them. Targets near the fuel bladder are only 3 to 4 m below the surface. The tunnel could go under them, but as a precaution they could be removed. An additional survey was run over a 30-m-wide swath from the ASTRO facility at the CARA site to the new elevated dormitory, a distance of approximately 800 m. This swath appears to be clear of any subsurface debris, except very near the dormitory. Surveys performed at several utility sites near the main station provided a general assessment of the dielectric properties of the firn, and tested the radar's ability to delineate subsurface features and potential hazards. Migrated, spatial images of the old clean air facility, the water well under development, and the several sewage sumps are presented. In general, the numerous vents, cables, antennas, etc., of the area clutter the profiles with diffractions that complicate interpretation of the data without prior knowledge of some features. The migrated images allowed approximations to be made as to the depths of sewage sumps, the water well and the old buried clean air facility.

Cover: View of the dome and arches at South Pole Station, looking at the main entrance.

For conversion of SI units to non-SI units of measurement consult *Standard Practice for Use of the International System of Units (SI)*, ASTM Standard E380-93, published by the American Society for Testing and Materials, 1916 Race St., Philadelphia, Pa. 19103.

CRREL Report 95-24

US Army Corps of Engineers
Cold Regions Research & Engineering Laboratory

Ground-Penetrating Radar Investigation of the Proposed Dome–CARA Tunnel Route and Utilities at South Pole Station, Antarctica

Steven A. Arcone, Wayne Tobiasson
and Allan J. Delaney

December 1995

Prepared for
NATIONAL SCIENCE FOUNDATION

PREFACE

This report was prepared by Dr. Steven A. Arcone, Geophysicist, Snow and Ice Division, Wayne Tobiasson, Research Civil Engineer, Civil and Geotechnical Engineering Research Division, and Allan J. Delaney, Physical Science Technician, Snow and Ice Division, Research and Engineering Directorate, U.S. Army Cold Regions Research and Engineering Laboratory. Funding for this research was provided by the National Science Foundation under Grant no. DPP-872 0063.

Technical review of this report was provided by Donald Garfield and John Rand of CRREL.

CONTENTS

ILLUSTRATIONS

Figure

Figure

Ground-Penetrating Radar Investigations of the Proposed Dome–CARA Tunnel Route and Utilities at South Pole Station, Antarctica

STEVEN A. ARCONE, WAYNE TOBIASSON AND ALLAN J. DELANEY

INTRODUCTION

Currently, a new facility is being built at South Pole Station, Antarctica, for infrared (IR) and millimeter wave (MMW) observatories operated by the Center for Astrophysical Research in Antarctica (CARA). This new research site is located about 200 m west of the skiway. Sensitivity to IR and MMW radiation is greatly enhanced by the absence of atmospheric water vapor and by very low telescope temperatures that reduce ambient IR noise; consequently, winter operations are necessary. A tunnel has been proposed to connect the CARA site with the main station. In it, personnel could move safely between the two places, which are about 1 km apart, even during the dark, cold winter-over period. A machine has been built at CRREL to excavate the tunnel, but the tunneler may be damaged if it encounters a large metal or wood object. Thus, the tunnel route must avoid any debris that has ended up in the snow during the 35 years that people have been present at the South Pole.

Commonly, magnetometry and low-frequency magnetic induction methods are used for metal detection. However, the nonmetallic nature of some of this debris, the 10-m depth of interest and the need to locate the objects accurately makes Ground-Penetrating Radar (GPR) the preferred method.

The objectives of our GPR surveys were 1) to locate any objects buried in the snow along the proposed route of the tunnel, 2) to determine the radar's ability to delineate known objects associated with the buried facilities near the main station, and 3) to assess the possible hazard of sewage sumps to the new water well near the main station. The surveys performed near the main station are discussed first, as they allowed establishment of the snow dielectric properties needed for estimating the depth of the objects in the tunnel route survey.

The tunnel route was surveyed using a GPR antenna transducer, operating at 400-MHz pulse center frequency, that was either pulled by hand or towed by vehicle along closely spaced, parallel transects covering a swath up to 60 m wide. The buried facility surveys were done at 100- and 400-MHz center frequencies. Some of the results were used to determine snow dielectric properties, which were needed to transform the GPR echo time delays into depth scales. As of this writing, there has been no drilling or excavation to verify the features of interest on the GPR records. Verification would be valuable.

GPR has been a common geophysical tool for subsurface exploration in snow and ice (e.g., Kovacs and Gow 1975, Kovacs et al. 1982, Arcone and Delaney 1987, Arcone 1991) and frozen soils (e.g., Annan and Davis 1976, Kovacs and Morey 1979, Delaney et al. 1991, Arcone 1992) because of the ease at which radio waves penetrate these materials. Commercially available, low-power, low-gain GPR systems are able to penetrate several meters in fine-grained permafrost, tens of meters in frozen sands and gravels, and well over a hundred meters in polar snow and ice. Vertical resolution is determined by the bandwidth center frequency of the pulse used. For antennas operating near 500 MHz, resolution is generally about 24 cm in dense snow, 20 cm in ice and less for dielectrically denser materials such as permafrost. This exceptional resolution has led GPR to become a popular device for characterizing utili-

ties and hazardous waste sites (e.g., Hanninen and Autio 1992, Pilon 1992), as most structures, subsurface debris, water and fuel spills, or the soil disturbances they cause, are strong radar targets.

This report discusses the use of GPR to detect such targets at South Pole Station, Antarctica. A companion report (Arcone et al. 1994) discusses additional surveys on the use of GPR in the vicinity of McMurdo Station, Antarctica.

RADAR EQUIPMENT

General operation

The radar utilized a Geophysical Survey Systems, Inc., SIR Model 4800 control unit, 100- and 400-MHz pulse center frequency antenna transducers, cables, a GSSI DT6000 digital tape recorder and a power supply. The control unit keys the transmitter on and off at 50 kHz (synchronized with the receiver), sets the scan rate (rate at which echo scans are compiled; generally 25.6 scans/s), scan time range and the time range gain to be applied to the scans. The transmit antennas radiate a broadband pulse lasting only a few nanoseconds (ns) at 400 MHz and about 15–20 ns at 100 MHz. Consequently, the antenna produces a low-gain radiation directivity pattern in ice or firn. Pulse shapes and directivity are discussed in detail below. A separate but identical receive antenna is employed because echoes can return from near-surface targets before the transmit antenna has stopped radiating. The received signals are converted by sampling into an audio frequency facsimile for filtering, amplification, digitization and recording.

Antennas

All antennas were flared and resistively loaded dipoles designed to produce a wavelet of about 2 cycles duration (Fig. 1). All wavelets have a 3-dB frequency bandwidth of about 35%. The 100- and 400-MHz characterizations refer to the approximate instantaneous frequencies of the radiated wavelets when coupled to snow or ice; higher frequencies result when radiating in air. The 400-MHz transmitter and receiver antennas are backshielded and housed in one unit (Model 3102, GSSI, Inc.) at a separation of about 15 cm. The transmitter produces an 8-W peak power excitation. A 100-MHz pair of transmit and receive antennas (Model 3207, GSSI, Inc.) was also used and they are of the same design, but housed in separate backshielded units so that the separation distance is variable.

Antenna directivity

The antenna beam pattern radiated into the ground must be considered when planning a survey of parallel lines so that subsurface coverage can be complete. Theoretical transmit radiation

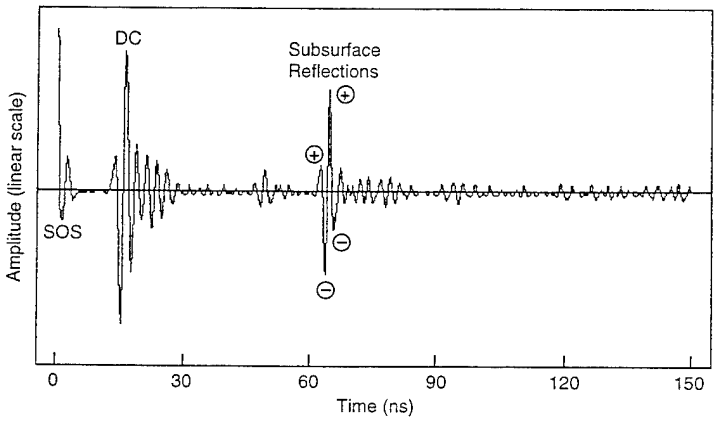

Figure 1. Short-pulse radar wavelet transmitted and received by 400-MHz GPR antennas. The wavelet shape is similar for both 100- and 400-MHz antennas. SOS is an artificial start-of-scan pulse and DC is the direct coupling between antennas (followed by resonance attributable to the snow cover). The large amplitude subsurface reflection is from a utilidor metal roof and the + – + – phase polarity sequence is characteristic of a conductive, or positive (i.e., higher than overburden), dielectric anomaly. The opposite sequence occurs for a negative anomaly such as a void.

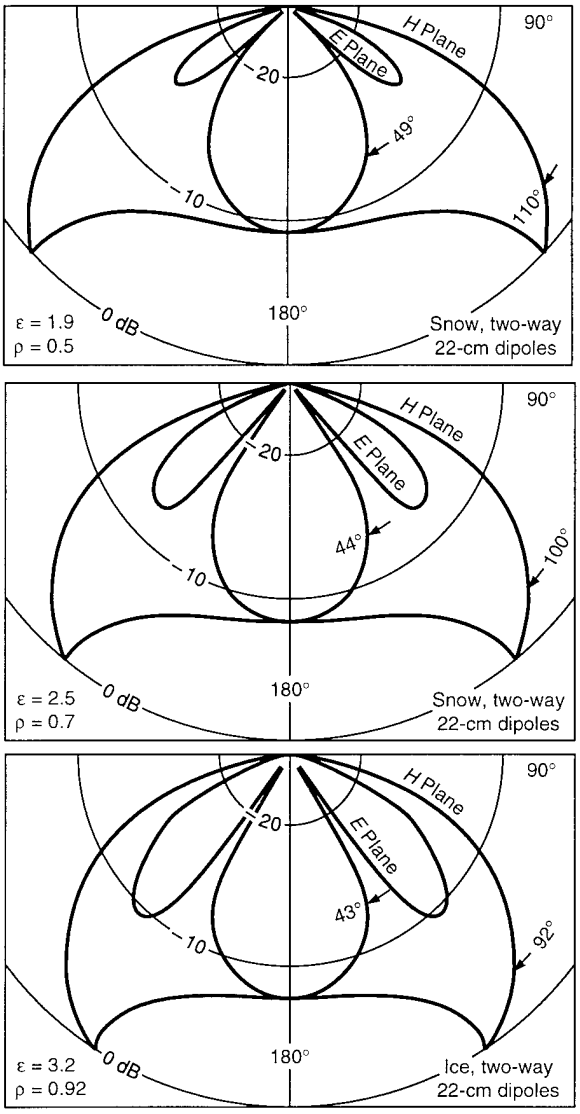

Figure 2. Radar transmit–receive two-way directivity pattern for a finite size dipole operating over snow of different densities ρ *and their corresponding dielectric constants* ε. *The directivity is much greater in the* E-*Plane, which is perpendicular to the direction of surveying. The 3-dB angular width in the* E-*plane gives an approximate base for calculating the antenna swath of sensitivity.*

patterns for point dipoles have been discussed by Annan et al. (1975) and Engheta et al. (1982). This theory shows the radiation to be directive with deep nulls and sharp lobes in planes parallel and perpendicular, respectively, to the antenna axis. These features occur in the angular directions $\psi = \pm \sin^{-1}(1/n)$ measured from vertical, where n is the real part of the refractive index of the ground medium. For solid ice, n = 1.78 and $|\psi|$ = 34°. This angle steadily increases to a value of 46.5° for snow of n = 1.38 (density 0.5; Cumming 1952).

The effective transmit–receive directivities for a theoretical model of our radar antennas (Arcone 1995) are shown in Figure 2. These patterns are the far field radar response to a point target that is isotropic, polarization insensitive, non-dispersive and located in three different media. The dielectric constants ε of the media are 1.9, an approximate value (e.g., Cumming 1952) for the upper layer snow at South Pole Station, 2.7 (dense snow) and 3.2 (ice). The patterns are more directive than those of a single antenna because of the multiplication of the identical transmit and receive directivity patterns. The patterns were computed for an antenna length of 22 cm, excited by a 2.5-ns (400-MHz) current pulse that progressively attenuates along the length of the antenna. The patterns are similar for the virtually identical, but larger, 100-MHz antennas.

The two-way directivity in the plane of the electric field (E-plane, which is the vertical plane containing the antenna and perpendicular to the ground surface), shows a main lobe and two weaker sidelobes. In snow of density 0.5 g/cm^3, the main lobe has a 3-dB beamwidth of 49° and the sidelobes are 5 dB weaker than the main lobe peak. Therefore, at a depth of about 5 m, the lateral coverage or "footprint" is determined by the main lobe and is about 4.6 m wide. The line spacing for the tunnel route survey averaged 2.8 m so that overlapping coverage was obtained. The unorthodox magnetic field plane (H-plane, which is the vertical plane perpendicular to the E-plane and the ground surface) pattern has two scalloped lobes whose peaks are about 9 dB above the peak E-plane intensity. An effective H-plane beamwidth is not simply characterized, but using the peak values in the 40° direction as a reference, the 3-dB width of each lobe is approximately 10°. This causes signal intensity to vary strongly along diffraction patterns generated when passing over discrete objects because profiling was done along the H-plane direction. This variation generates "noise" during migration. Migration is a signal processing procedure used for resolving diffractions to improve the spatial imaging of the radar data. It is used later and discussed below.

FIELD PROCEDURES AND DATA PROCESSING

Field procedures

We established transects over facilities near South Pole Station by placing orange plywood diamonds in the snow at set intervals along lines

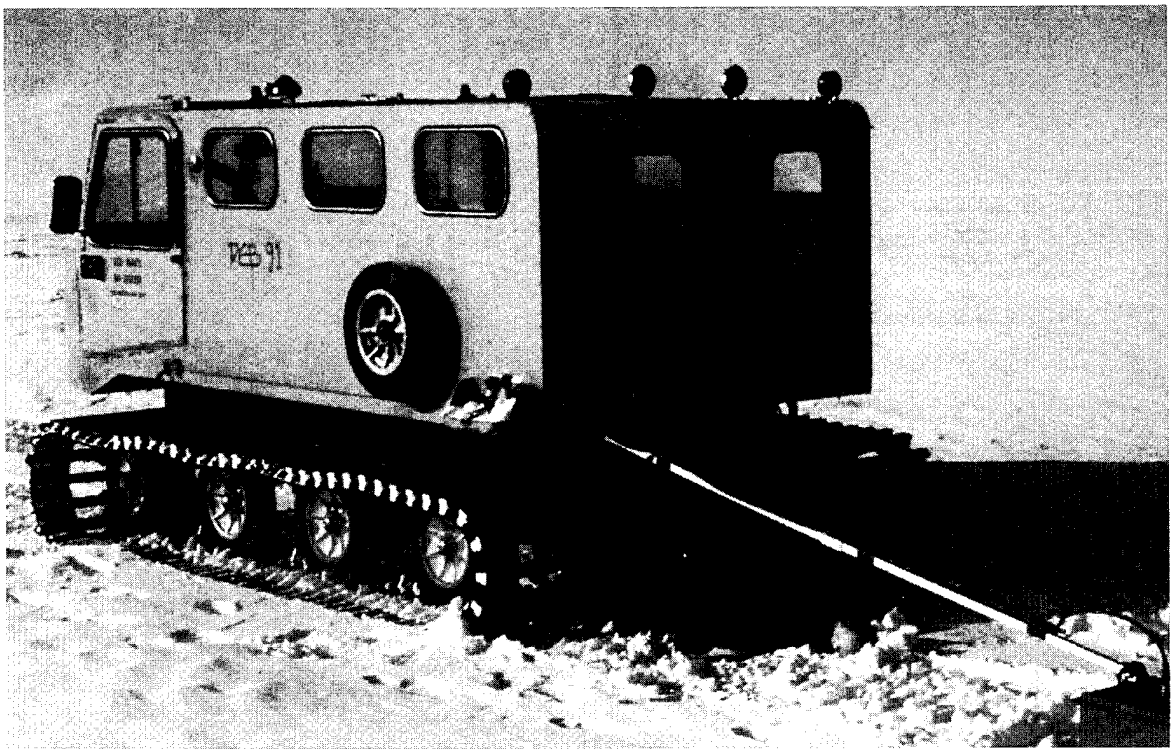

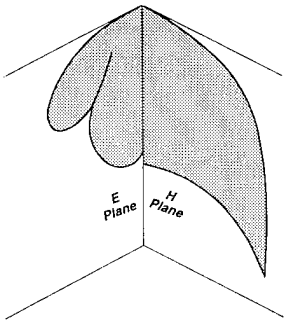

Figure 3. 400-MHz antenna transducer unit in tow behind a Spryte tracked vehicle. The transducer contains the antennas and transmit and receive electronics. No reflections from the Spryte were apparent in the records. Spryte speed was generally about 5 m/s. Also shown is the two-way radar antenna directivity patterns in firn, both perpendicular (⊥) and parallel (| |) to the profile line direction. The perpendicular pattern covers a subsurface swath extending about ±25° to the sides of the antenna.

to be surveyed and then slowly dragging the antennas by hand from diamond to diamond. Transects along the proposed tunnel route were done by slowly dragging the antennas over the surface behind a Spryte tracked vehicle (Fig. 3) at 8–13 km/hr (5–8 miles/hr) along similarly marked lines. Differences in record length ascribable to changes in towing speed between diamonds or flagged bamboo poles were compensated for by computer processing. All surveys were performed with the antennas polarized perpendicular to the transect direction so that the stronger amplitude H-plane pattern was in the line of the transect. The spacing of the tunnel lines sometimes varied by a few meters to avoid surface obstacles. Thus, the exact position of targets located is not known. Event markers were placed electronically on the tunnel records at known positions along each traverse. The transect line spacing averaged 2.8 m, slightly more than the 2.5-m width of the vehicle's tracks.

Data recording, filtering and processing

All data were recorded in scans of either 512 or 1024 8-bit words for later processing by dedicated software (Galinovsky and Levin 1990). Horizontal (i.e., over distance or equivalently, many scans) frequency filtering mitigated near-surface ringing from the direct coupling between antennas, and vertical (i.e., over time, or equivalently, along one scan) filtering mitigated dc gain variations resulting from inconsistent antenna–ground coupling. Data are displayed as consecutive scans in a distance-vs.-echo-time arrangement (known as a "time section") (Fig. 4) for which several schemes for displaying signal amplitude are available. Only selected sections of the tunnel survey will be shown owing to the large amount of data.

Translation of echo time delay t from a target into the depth d of the target is generally based on the simple echo delay formula

$$d = ct/2n \qquad (1)$$

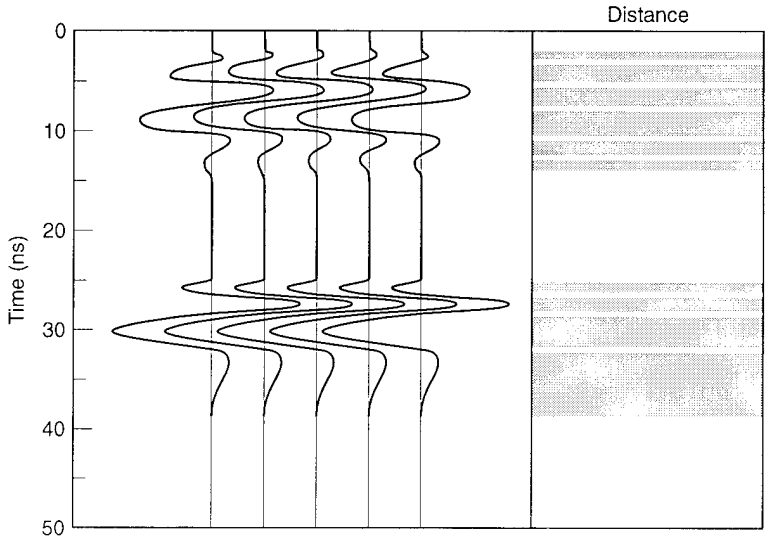

Figure 4. Wiggle trace display (left) of a series of scans received as the antenna moves over a short distance, and the equivalent line intensity display.

where d is measured in centimeters, t in nanoseconds and c is the speed of electromagnetic waves in a vacuum (30 cm/ns). The quantity n is often replaced by $\sqrt{\varepsilon}$; where $\varepsilon = 3.2$ for ice and about 1.9–2.2 for most of the near-surface snow encountered. The factor of two in eq 1 accounts for the round trip propagation path of the pulse and applies only to reflections from horizontal interfaces or to scattering from point sources. Equation 1 can be applied to several layers successively if n is known for each layer and the time delays to each layer interface are easily picked from the record.

Proper transformation of a standard radar distance-vs.-time profile into a more useful spatial image of distance vs. depth is achieved by a computational process known as migration, commonly used in seismic data processing. Migration is not necessary where reflecting horizons gradually change depth with distance, but should be used where reflections strongly slope or curve and may be masked by strong diffractions from local targets.

Migration is achieved by many methods. The most common, the Kirchhoff diffraction summation method (e.g., Yilmaz 1987), is used in these studies. Migration requires a wave velocity (or value of n) for each material type encountered, but we used a one-layer approximation for the snow; i.e, we assumed that the snow is a homogeneous matrix of constant n and containing embedded anomalies. In fact, n increases gradually with depth. We used a migration refractive index value, n_m, calculated from matching the hyperbolic diffractions with a model hyperbola. The values obtained, calculated at an accuracy of about ±4%, produced good migrations, as judged by the collapse of the diffraction hyperbolas to a small area, and can therefore be considered as nearly the average refractive index.

All time section profiles to be migrated had to be compressed (i.e., stacked, wherein each scan is replaced by the average of several scans symmetrically placed about it) so that an adequate migration aperture (number of scans processed at one time) could be obtained to cover an entire diffraction. The resulting migration was then stretched by interpolating between scans to give a reasonable ratio between depth and distance scales. Details of the migration algorithm and the probable effects of antenna directivity upon it are discussed in Arcone et al. (1995).

Migration is used primarily in the studies of the dome facilities to help us interpret subsurface structure. The diffractions that emanated from the many targets encountered along the proposed tunnel route are not migrated because they themselves are evidence of target presence (their obscuration of snow layering is of no interest) and their amplitude and waveforms may supply information about their material nature.

RESULTS AND DISCUSSION

Station site surveys

The objectives of these surveys were twofold: to obtain values for the effective dielectric constant of the firn (i.e., snow over a year old, but not yet com-

pressed into glacial ice) over various depths, and to locate or delineate subsurface facilities and utilities, or both. Figure 5 shows the general layout of South Pole Station and the surveys. The facilities discussed are the present water well, several sewage sumps produced over the years (indicated as sump 1, sump 2 and far sump), a utilidor and the buried Old Clean Air Facility (OCAF). Each survey line is lettered (e.g., FG) with the alphabetical order indicating the direction of the line. Several transects are indicated at each site, but not all are presented in this report as some did not traverse the features of interest. One Wide-Angle Reflection and Refraction (WARR) line (transmitter and receiver antenna offset constantly increased: on the diagram) was made near the OCAF to evaluate the refractive index of the surface snow. Dielectric information was gathered from all surveys. The weather during all profiles was clear with light winds and temperatures between –13 and –26°C, which necessitated placing the radar control unit within an insulated box.

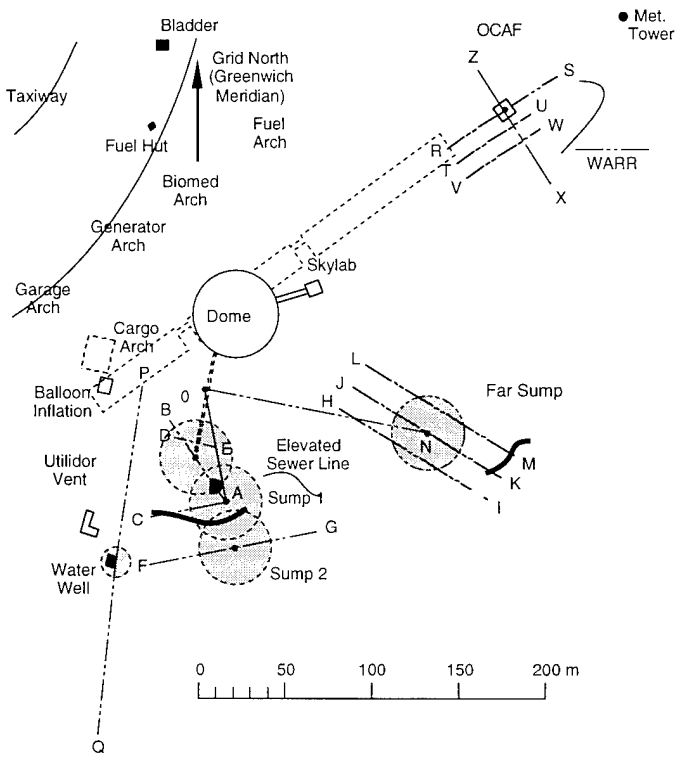

Figure 5. Layout of facilities and radar survey lines (end points alphabetically marked) at South Pole Station, January 1993. Line marked WARR is a wide angle survey.

Near the surface, snow density is approximately 0.35 g/cm^3 and increases to a firn density of about 0.8 by 100 m depth (Bogorodsky et al. 1985). About 15–20 cm of new snow accumulates each year at the South Pole. The snow that was on the surface during the beginning of the International Geophysical Year (IGY; 1957) when the South Pole was first permanently occupied was about 4–5 m below the surface at the time of our surveys. Over the years objects have been buried. Some objects are even deeper, since pits were dug to bury waste as far back as the IGY. In the early 1970s, a second station was built 1.4 km from the original IGY station, creating heavy vehicular traffic between the two stations. This created a hard, compacted layer that, at the time of our surveys, was 3 to 4 m below the snow surface. That traffic area crosses routes proposed for a tunnel and is evident in many of the radar surveys. Extra snow accumulation around the main station places that layer 4 to 5 m deep there and it is also visible in the radar records. However, since all snow above it has since been compacted by annual snow control operations, other layers are also evident in the radar survey.

Also apparent in all the records are diffractions unrelated to the feature of interest. We expect that these "clutter" events are generated by buried objects including trash, spills, vents, cables and antennas.

Metal utilidor

The metal utilidor leading south from the main station (Dome in Fig. 5) was first surveyed (line DE) to establish a calibration value for the snow velocity since the exact depth (5.65 m) from the snow surface to the crown of the metal tunnel was known. The utilidor tunnel itself is 2.0 m high (Fig. 6). Figure 6 also shows the radar profile, acquired with the 400-MHz transducer. The prominent but distorted hyperbolic diffraction under the centerline symbol and whose apex is at 49-ns delay is the response to the utilidor roof. The reflected wavelet at the apex is the large reflection shown in Figure 1. Several other hyperbolas appear in the profile and are generated by buried objects whose depth and placement relative to the vertical plane of the survey line is not

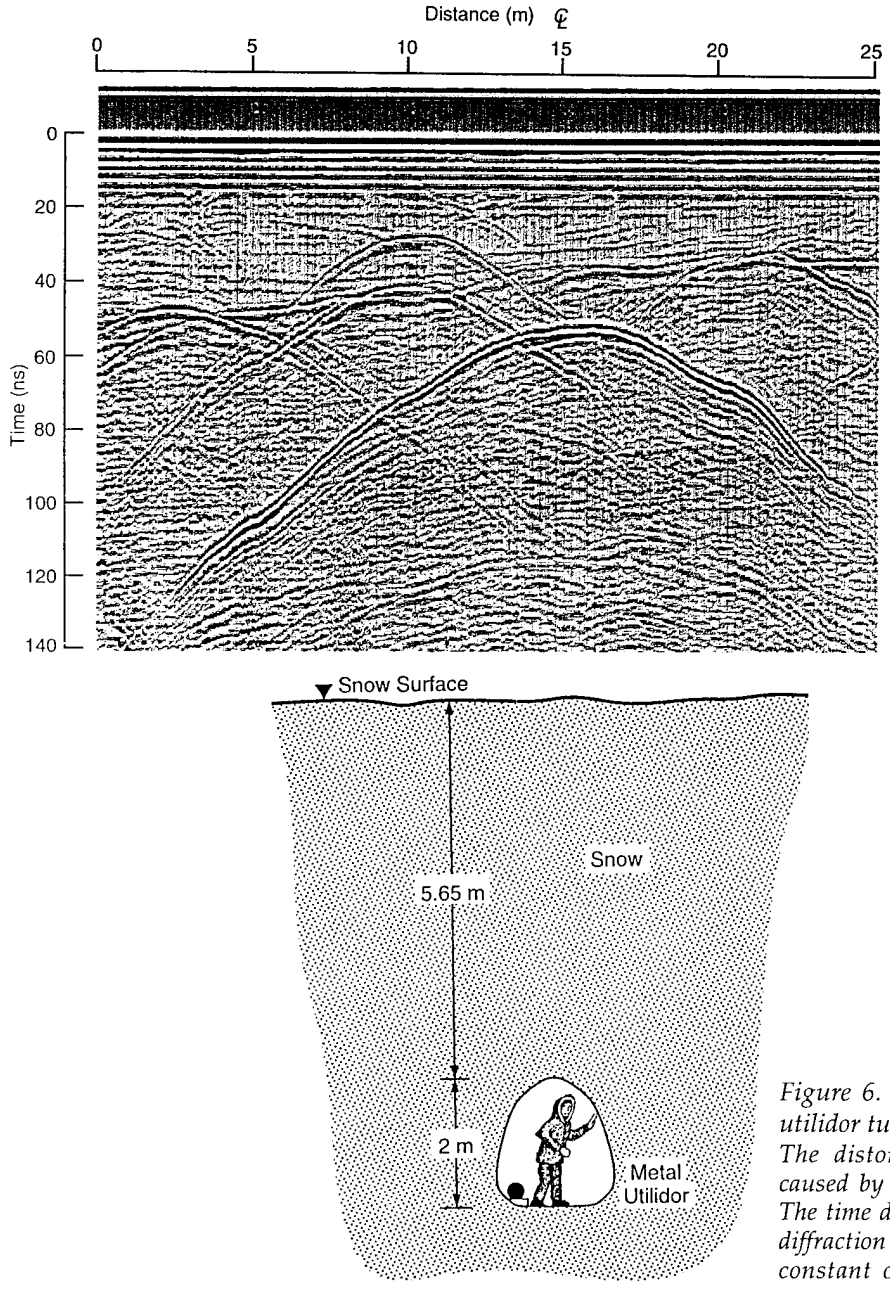

Figure 6. 400-MHz profile of the metal utilidor tunnel along line DE in Figure 5. The distortions in the diffractions are caused by uneven antenna towing speed. The time delay to the utilidor roof and the diffraction itself correspond to a dielectric constant of 1.57 and a snow density of about 0.34 g/cm^3.

known. The distortions in the diffractions are caused by uneven towing speed. The more uniform left limb of the utilidor diffraction can be matched with a theoretical curve generated with a refractive index $n_m = 1.26$ ($\varepsilon = 1.57$), which is close to the values (1.30, 1.69) corresponding to the velocity arrived at using the utilidor depth and time delay. These values correspond to snow density of 0.34–0.37 g/cm^3 (Cumming 1952) and are slightly less than other values obtained at the South Pole and discussed below.

Old Clean Air Facility (OCAF)

This facility has been abandoned and is known to be under several meters of snow; our purpose here was to find it. A 100-m survey line (line XZ in Fig. 5) that apparently traversed the roof is shown in Figure 7, along with its migration. The data were horizontally filtered and compressed sufficiently to allow the maximum migration aperture (127 scans) permitted by the software to cover an entire diffraction. All the diffractions fit a model hyperbola generated by a migration velocity cor-

responding to an $\varepsilon = 1.93$, which corresponds to a firn density of 0.5. The correctness of this value is revealed in the migration, which transforms the unmigrated data into several horizontal surfaces.

The unmigrated data of Figure 7 reveal a linear coherent reflection at about 55 ns delay, and many diffractions of which two, centered at 15 and 29 m, are very prominent. The migrated data show the linear reflector to be between 17 and 28 m. We presume that a major part of the linear reflection is the roof at a depth of about 5.5 m. The facts that 1) the 11-m distance is much greater than the original roof dimensions (6.4 × 7.3 m; diagonal length = 9.8 m) and, 2) that there are many more diffractions originating at 60 ns towards point Z, suggest that there is more structure buried. The apexes of the prominent diffractions are at about 40 ns and the migrated data resolve these diffractions into two apparent columns. The strong diffraction originating at about 15 m collapses to a horizontal surface (i.e., coherent reflection) about 2 m wide at 4 m depth. The diffraction at 29 m distance also collapses to a coherent reflection at about 4 m depth, but it is not as linear. These diffractions could be responses to metal pipes placed to mark the location of the

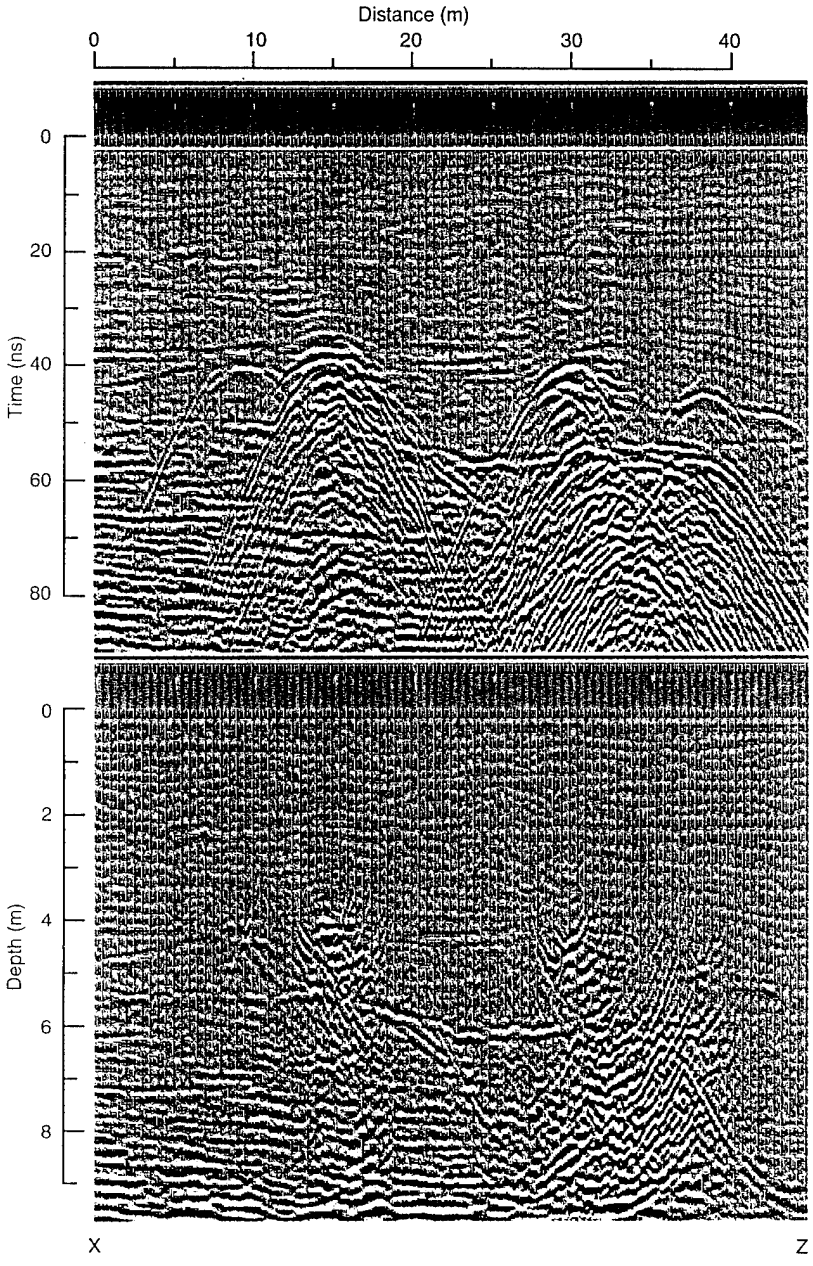

Figure 7. 400-MHz profile (top) and its migration along line XZ that crosses the old clean air facility. Many of the diffractions in the top profile have collapsed into discrete events in the migrated section. The linear reflector provides convincing evidence that the building has been located.

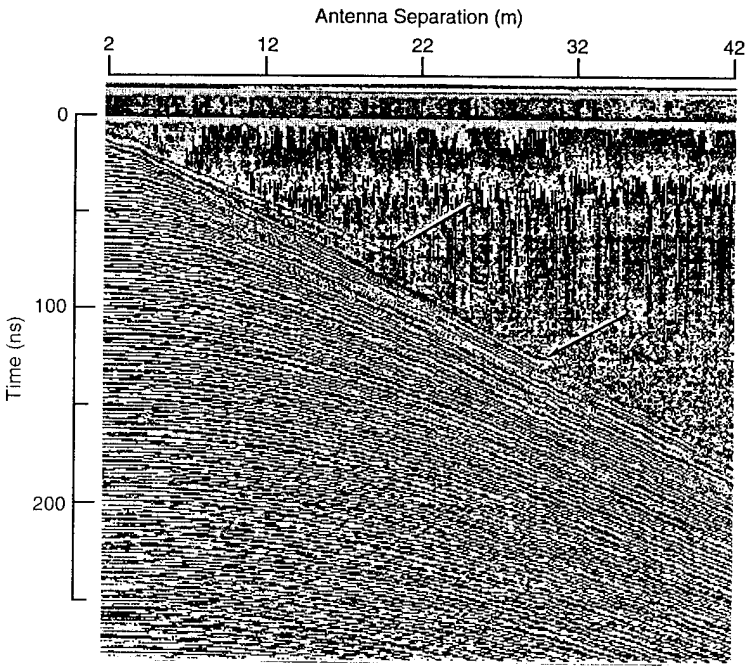

Figure 8. Wide angle reflection and refraction profile performed at about 400 MHz near the OCAF. Arrow 1 points to the directly coupled air wave, followed by the directly coupled ground wave (arrow 2). All other events become parallel with the ground wave. The slope of the ground wave corresponds to n = *1.28, equivalent to an approximate snow density of 0.33 g/cm^3. Bright spots and noise bands are artifacts of the automatic gain control used to amplify the weak air wave.*

buried building after it was abandoned in the mid-1970's.*

The migration dielectric constant of 1.93 is an integrated value. The fact that ε increases with depth is demonstrated by the results of a WARR profile taken near the site (Fig. 8). The WARR used two Model 3102 units, one as a transmitter and the other as receiver; only the transmitter was moved. At the expense of noise amplification, automatic gain control was applied to this record to make visible the first event, the weak direct air wave coupling. The time–distance slope of the direct air wave coupling gives a velocity of 31.0 cm/ns, an error of about 3% over the actual value of 30 cm/ns. The ground wave slope gives a value of n = 1.28. This value of n corresponds to a near-surface density of about 0.35 g/cm^3 and, therefore, represents only the upper layers of snow. All subsequent subsurface reflections become parallel with the ground wave as they refract into the faster near-surface media; thus, refractions spend more time near the surface.

New water well and nearby sewage sumps

The new water well is located just south of the main station (Fig. 5). It was being formed during our visit. First, a shaft was melted with hot water down through permeable snow to a depth of about 60 m where water began to pond. This water was brought up, heated and returned to enlarge the pool. As the pool grew, a cavity was created above it since the meltwater occupies less volume than the dense snow it replaces. At the time of the survey, the surface of the pool was 70.1 m (230 ft) below the snow surface and its diameter was thought to be approximately 9 m (30 ft). The air bulb began at about 60 m depth and so there was approximately 10 m of air space above the water surface.

Three sewage sumps located nearby are labeled utilidor vent, sump 1 and sump 2 on Figure 5. The objective here was to determine if the radar could detect these sumps and, if possible, measure their lateral extent, known to be about 21 m. We also hoped to obtain an effective dielectric constant of deeper firn by using the diffractions from the well, whose depth was known.

A 100-MHz time section profile along the line PQ (Fig. 5) across the well is shown in Figure 9. The 100-MHz transducer was used because the sampling rate was sufficient to reproduce the signals at the necessary time range. The slight surface elevation difference of about 2 m from the north to the south end of the profile was inconsequential in view of the large time range used to reach the well. The wide hyperbola peak at 762-ns time delay is the response to the water in the well, which is a prominent target with large radar cross section and a positive dielectric anomaly (higher dielectric constant than that of the snow). This is consistent with the phase polarity of the response; a response to the hemispherical air bulb, which has a low radar cross section, would have the opposite phase because it is a negative dielectric anomaly.

* Personal communication with A. Hogan, CRREL, 1995.

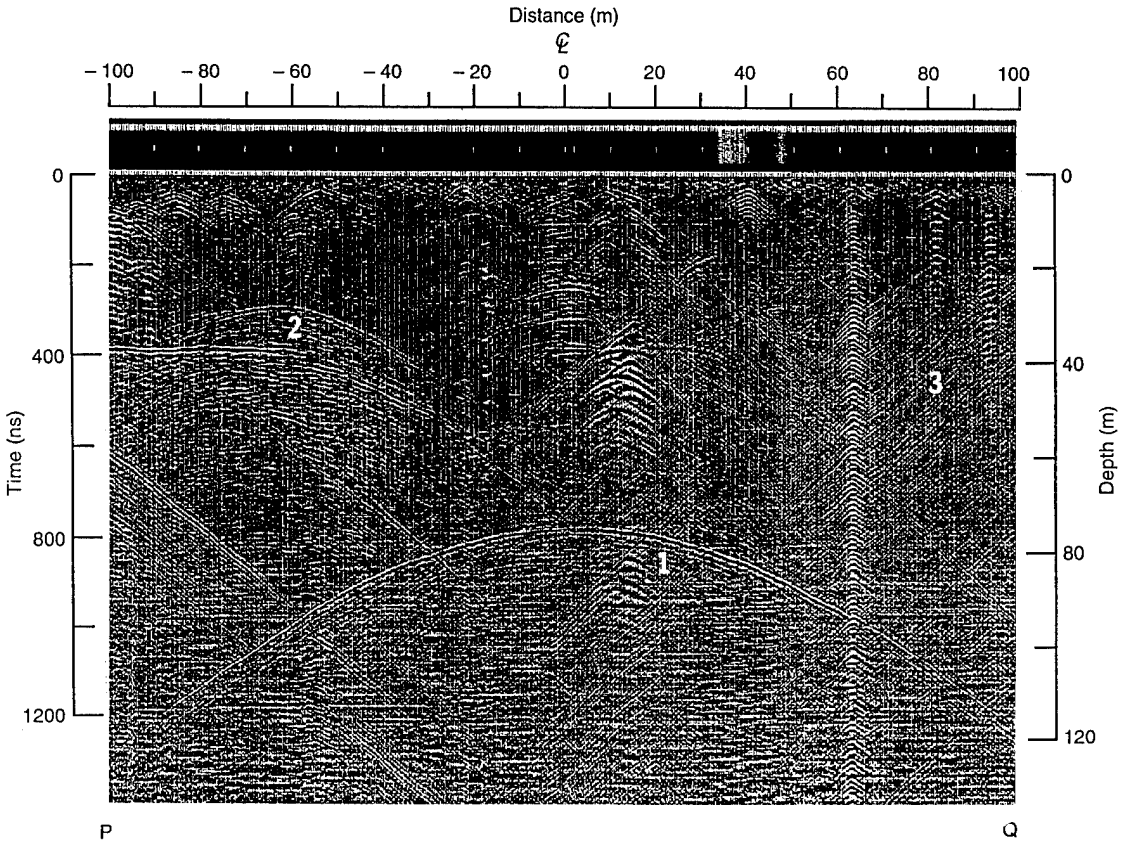

Figure 9. 100-MHz time section profile across the water well, the depth of which was 70.1 m. The asymptotic slopes of the hyperbolic diffraction from the well (1) give an $n_m = 1.59$*; the slopes of the more shallow hyperbola (2) from an unknown object give* $n_m = 1.46$*; and the slopes of the resonant waves (3) generated by surface objects give* $n_m = 1.36$.

A refractive index of 1.59 ($\varepsilon = 2.53$) gives an almost perfect hyperbolic fit to this diffraction, and corresponds to an overburden average density of about 0.7 g/cm^3. Alternatively, given the time delay and the measured depth to the water of 70.1 m, the effective refractive index for the firn overburden is determined to be 1.63 ($\varepsilon = 2.66$). Although the estimated bulb diameter is 9 m, there is no evidence (e.g., two hyperbolae) of separate diffractions from each end of the bulb, as the temporal displacement of their asymptotes would be over 80 ns at the ends of the profile. Therefore, the diffraction itself, centered exactly at the center of the water well, is primarily a response to the complete well surface, but undoubtedly modified somewhat by the air bulb.

There are many other events in Figure 9, the origins of which are not known. The area was extremely cluttered. Events with a slope corresponding to a refractive index near 1.3 are either surface or near-surface objects. Event 2 in Figure 9 is a hyperbola that gives a refractive index of 1.46 (density = 0.55 g/cm^3 at an approximate depth of 29.5 m, assuming the object was directly beneath the profile). The slopes of the linear sloping events throughout the record (e.g., event 3 in Fig. 9) give a refractive index of 1.36 (density = 0.45 g/cm^3). The accuracy of these measurements is about 4%, based on the error of making a best fit to the diffractions.

A migration of the water well profile is shown in Figure 10. The time section profile had to be compressed by a factor of two (subsequently expanded) so that the migration aperture could encompass most of the water well diffraction. The migration collapses the hyperbolic diffraction from the well to a segment approximately 16 m wide. This is wider than the estimated bulb diameter of 9 m and may be partly an artifact of the algorithm and the finite pulse width, as theory (Yilmaz 1987) shows that a perfect diffraction hyperbola generally collapses to this finite sized form rather than to a singular point. For estimating the encroachment of the sumps, we have assumed that the current diameter of the water well could be as great as 16 m.

Three sumps in this area, sump 1 and sump 2, and one below a utilidor vent south of the dome,

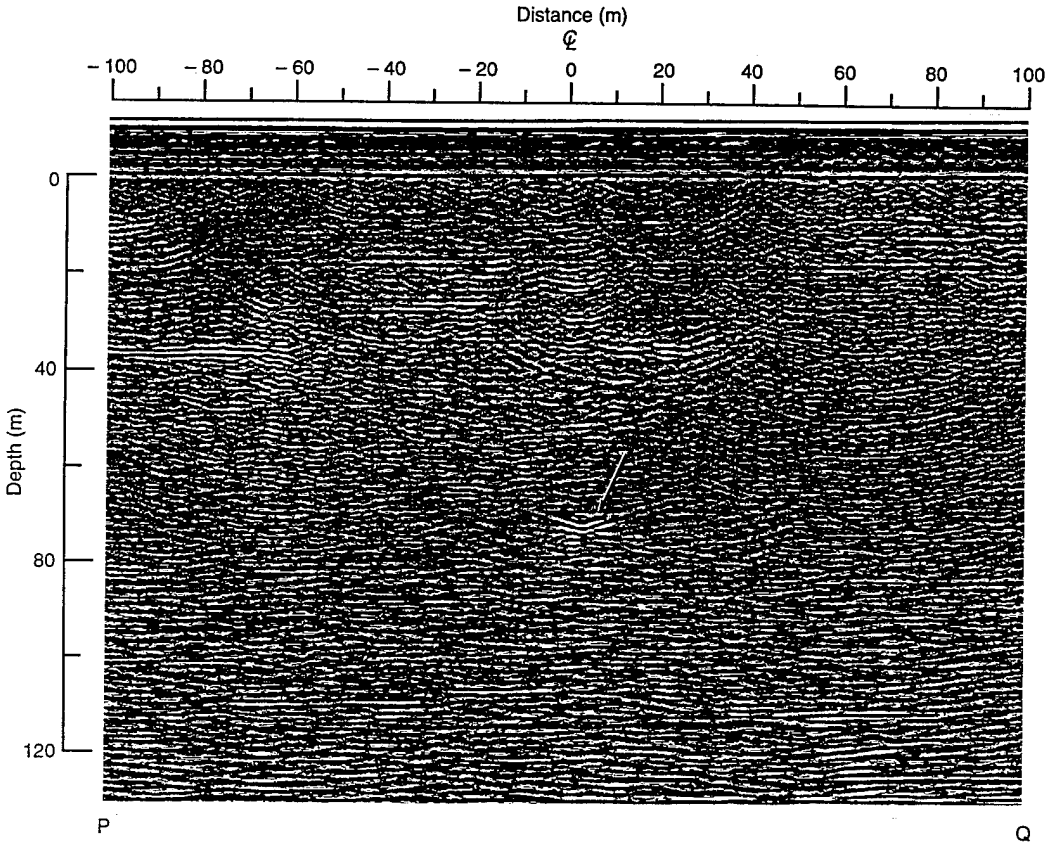

Figure 10. Migration of the water well profile seen in Figure 9. The central bright spot at 71-m depth (arrow) is the water well and its width may be ascribable to a migration algorithm artifact because the diffraction is almost a perfect hyperbola and should migrate to a point. More shallow events in the profile are improperly migrated because of changing velocity with depth.

are marked in Figure 5. At the time of the survey, sump 1 was believed to look as depicted in Figure 11, which is based on prior CRREL and Metcalf and Eddy (M&E), Inc., measurements there and CRREL studies of similar sumps in Greenland. The surface of the central liquid pool was measured at 17.4 m below the snow surface during our surveys and the zone of sewage-contaminated 0°C snow was found the year before to extend radially about 21.3 m. At the extremities of the sump, the depth to the sewage-soaked material increases about by 3 m. This sump is in use and thus there is a central liquid pool and water in the upper portion of the contaminated snow.

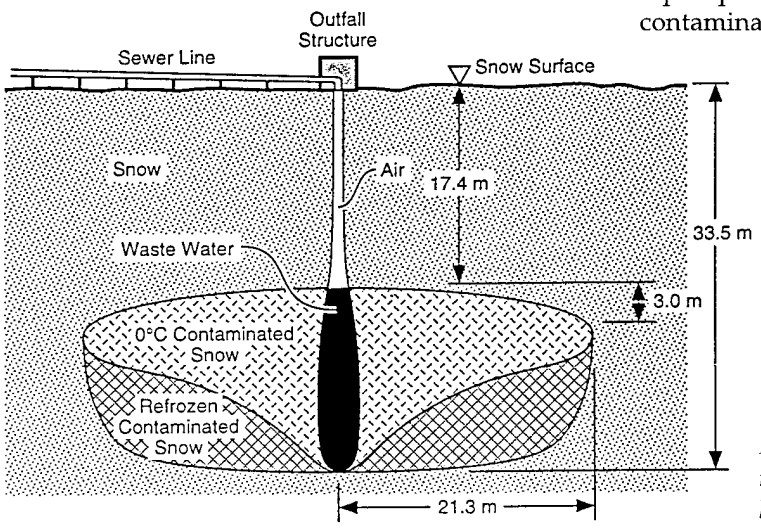

Figure 11. Two-dimensional depiction of the disposition of sewage within sump 1 at location A in Figure 5.

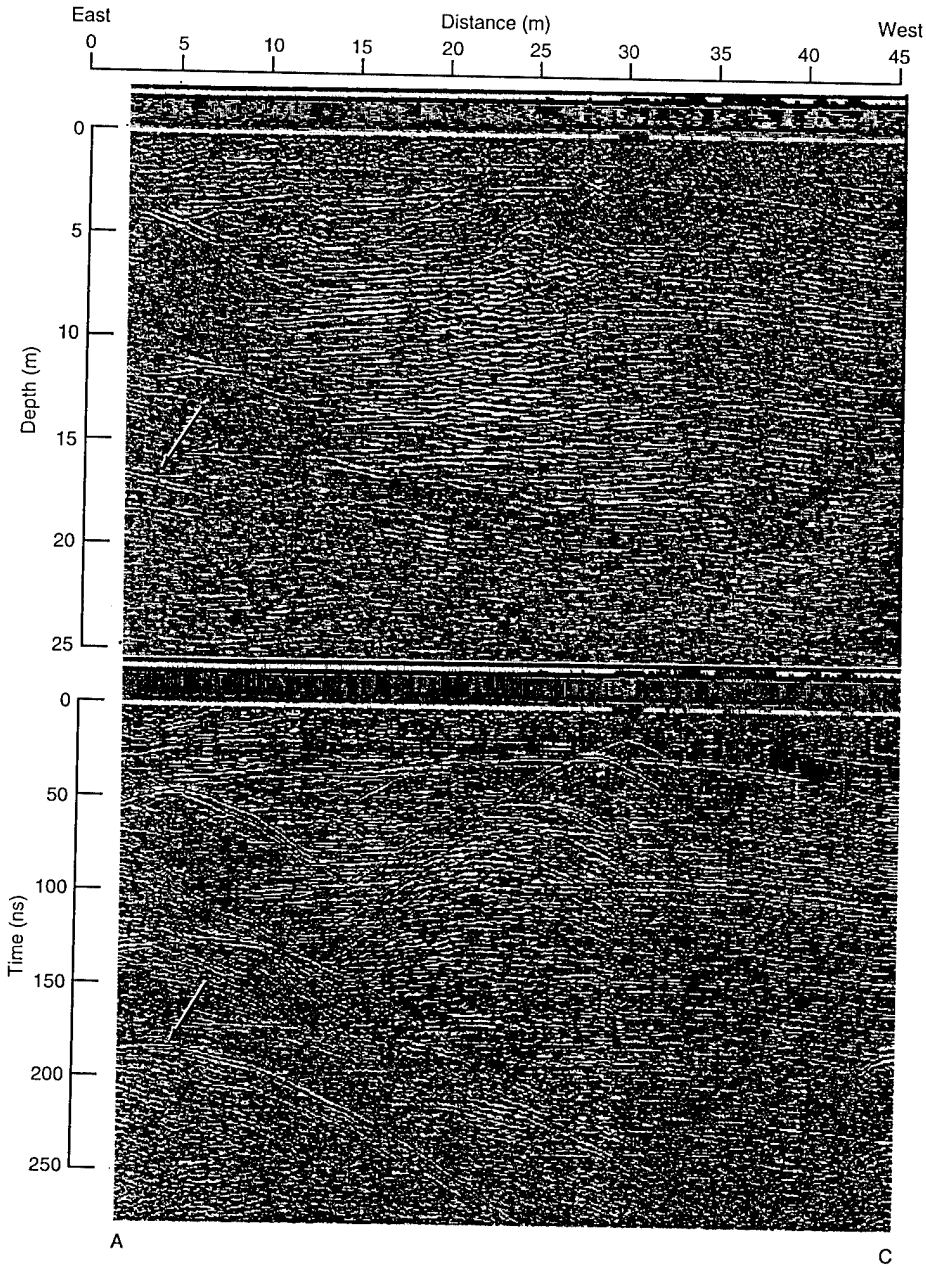

a. Line AC, which runs west from the sump 1 area. Arrows point to the response of the sump at a depth of about 17 m.

Figure 12. 400-MHz time-section profiles (bottom) and their migrations.

The area marked sump 1 was profiled along two lines (AB and AC) as shown in Figure 5. These profiles along with their migrations are shown in Figure 12. The migration used a value n_m = 1.55, obtained from the sump 1 diffractions, to calibrate depth. The time section in Figure 12a (bottom) along line AC shows the diffraction response of the sump (arrow) to originate at an approximate depth of 17 m. The migration of this profile (Fig. 12a, top) shows the sump response to extend only about 7 m in the westerly direction, considerably less than the 21 m expected on the basis of penetration rate measurements of holes melted with an electric heater some time ago.

The time section profile in Figure 12b (bottom) along line AB starts at the center of sump 1 and passes near the utilidor vent at about 29 m and over the sewage sump centered about there. As shown in Figure 12a, the sump 1 response (arrow A) occurs at a depth of about 17 m and seems to extend only about 7 or 8 m northward. The diffraction response, which we believe is the utilidor roof

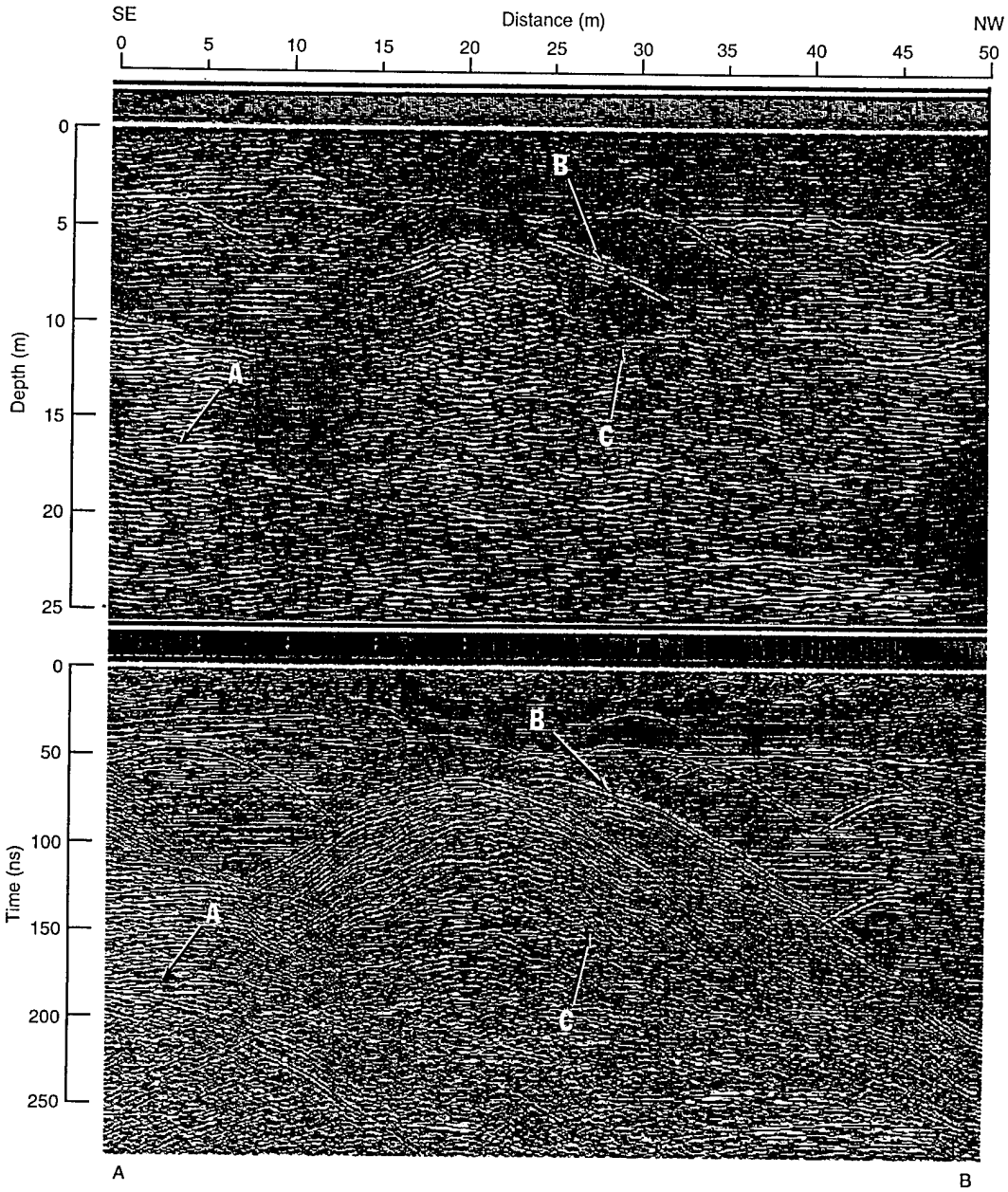

b. Line AB, which runs from the sump 1 to the utilidor vent in Figure 5. Arrow A points to the sump 1 response and arrow B to the probable response of the utilidor vent. The vent response migrates to a slope, which indicates increasing distance from the utilidor. The slope originates at 25 m and may indicate a positional error. The sump response at the vent is probably the diffractions indicated as C. The spread of sewage in both sumps suggested by the migration is believed to be far too small.

Figure 12 (cont'd).

(arrow B), occurs at a delay of 70 ns and, given a depth of 6.9 m from our verification survey, corresponds to an n_m = 1.52. Although this value agrees well with our migration refractive index of 1.54, snow nearer the surface is of less density, as we have seen above, and is more likely to have an n = 1.3. This would place the actual distance to the roof at about 7.7 m at the 29-m distance, which suggests that we may have been off the center of the utilidor. In addition, the time section migrates to a one-sided dipping reflection, rather than a point, as would happen for a fixed target (the roof) whose distance increases from the radar receiver. The difficulty with this explanation is that the dipping reflection appears to originate at a 25-m distance. Resolution of this problem is not possi-

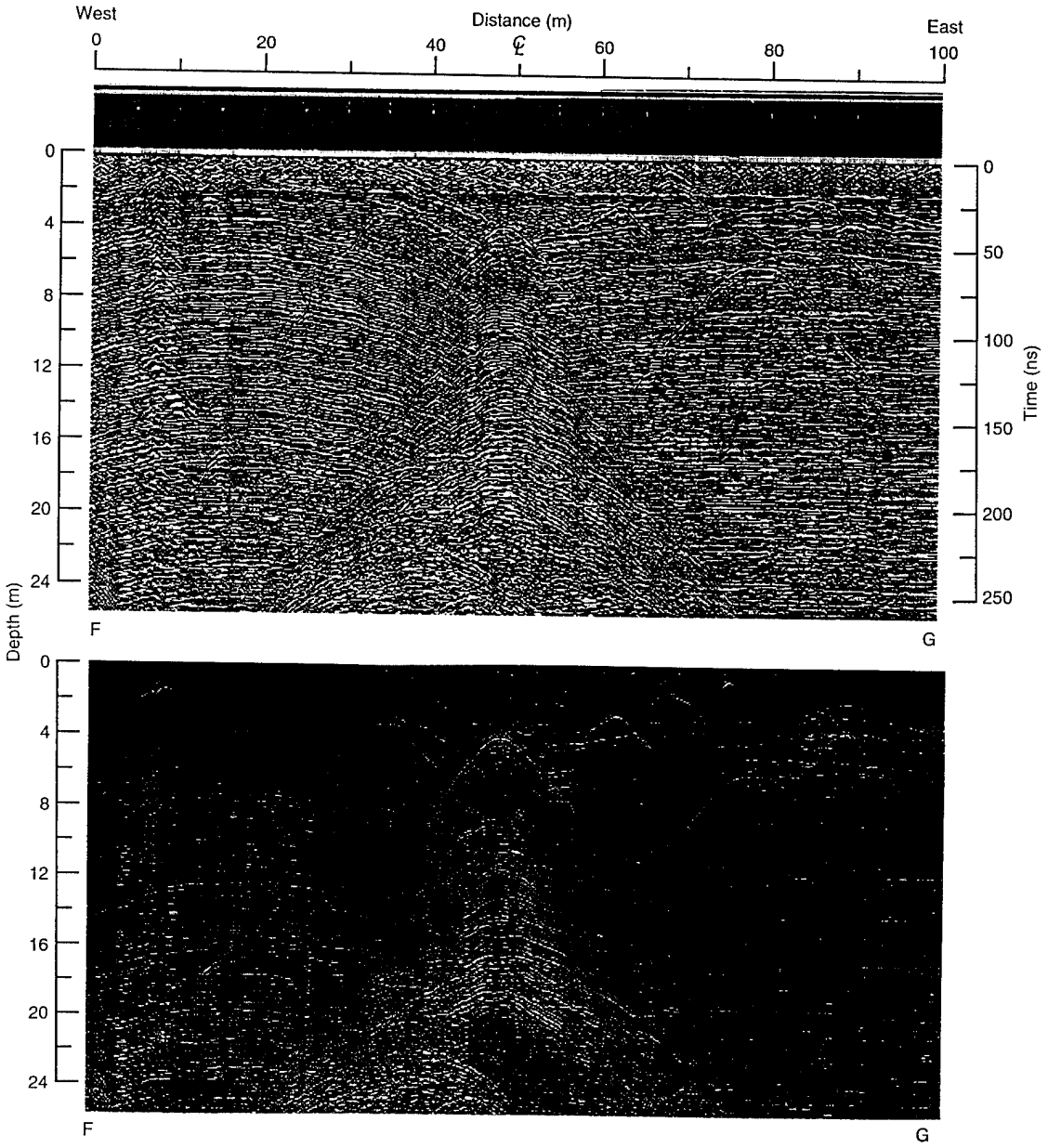

Figure 13. Two versions of the 400-MHz profile recorded at 300 ns across line FG over sump 2. The sump is centered at the 50-m distance. The bottom profile represents an estimate of the actual reflective strength throughout the sump and shows greater diffraction intensity below 12 m where frozen sewage begins. The later diffractions are strong enough to make their asymptotes visible. The top profile equalizes the intensity of all events and reveals the density horizons that subside toward the sump.

ble without better knowledge of our exact antenna location, near-surface snow density structure and any debris or other structures that may exist above the roof.

The depth to contamination at the sump below the utilidor vent had to be 9 m or less, since some time ago that sump had filled to the level of the floor of the utilidor. The depth could even be less, since sewage was discharged up the utilidor about 13.4 m toward point O and could have raised the level of the contamination in this area. We believe that the response to this sewage is event C in Figure 12b. The radar data migration suggests that the radius of the sump below the end of the utilidor is about 5 m, but we expect that it is much larger.

Sump 2 was traversed from west to east along line FG (Fig. 5). The center of the sump 2 area is approximately 70 m from the center of the water

well. Prior CRREL and M&E measurements have shown the depth to contamination at the center of sump 2 to be approximately 12 m. Sump 2 is probably similar to the depiction in Figure 11, with a radial extent of about 21 m and a maximum depth of about 35 m. However, since this sump has not received warm sewage for some time, no liquid exists within it.

The 400-MHz time section profile over sump 2 between points F and G is shown in two versions in Figure 13. All of the hyperbolic diffractions in the profile can be matched well using a refractive index of about 1.54. We used this value to calibrate the depth scale, and it corresponds to an average snow density of about 0.65 g/cm^3. The signal intensities within the bottom profile are approximately proportional to the actual reflectivity throughout the sump because signal loss with range is compensated for by the radar system Time-Range-Gain (TRG) function. Several closely spaced diffractions, originating over the center of the sump area, begin at an apparent depth of 4 m and continue throughout the depth of the record. Within these diffractions lies the stronger responses to the frozen sewage at just over 12 m depth. The many diffractions that originate below 12 m are probably from deeper portions of the sump, which is expected to extend to a depth of about 35 m. These diffractions are so strong that their asymptotes are highly visible, a consequence of the off-axis strengthening of antenna directivity shown in Figure 2.

The top profile of Figure 13 equalizes the gain throughout the record so that all events are equally apparent, especially those from the density contrast interfaces, which appear to subside toward the sump. This subsidence is consistent with known increases in snow consolidation from warming in the vicinity of such sumps. Snow consolidation is also apparent from the refractive indices measured at sumps 1 and 2; the values of 1.5 to 1.6 over the 16-m depth are higher than maximum values (1.4) found over similar depths along the tunnel survey.

A migration of the central section of this profile is shown in Figure 14. Some of the peak signal strengths along the profile scans are amplified to bit saturation to allow us to view the deeper returns. The migration shows a coherent horizon at about 14 m depth and then reflections that spread asymmetrically to an approximate width (diameter) of 25 m at a depth of about 16 m. The sump 2 region seems to extend about 15 m to the west, but this sump is known to be refrozen and to extend radially about 20 m towards the water well. Therefore, we conclude that the contaminated firn beyond a 15 m radius did not produce detectable reflections.

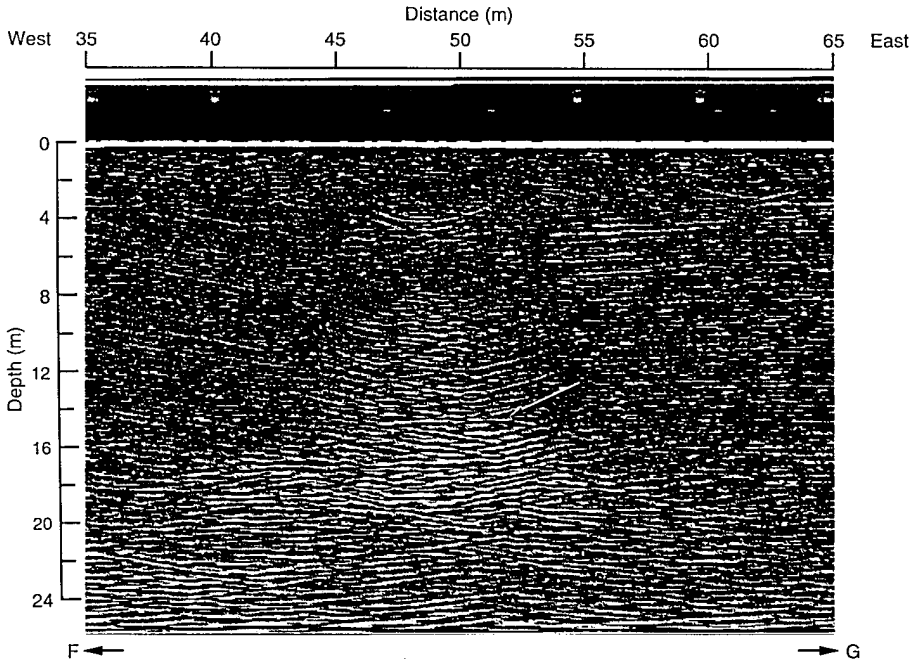

Figure 14. Migration of the central section of the sump 2 profile using a migration velocity based on n_m = 1.54 (density 0.65). The section indicates that the sewage spreads to an estimated width (diameter) of 25 m, 15 m of which is towards the water well. Arrow points to a coherent reflection at about 14 m depth.

In summary, the contaminated areas of sumps 1, 2 and the sump below the utilidor vent seem well isolated from the water well. The radar indicates about an 8-m radius for the water well and a spread of about 15 m for the sump 2 contamination toward the well. This leaves more than 45 m separation between the well and the nearest contamination. Since the well bulb is below the contamination, the radar suggests that there is about 55 m separation between the nearest contamination and the water well itself. However, since probes indicate that the radii of the sewage sumps are about 21 m, not 15 m, it is likely that the actual separation is closer to 50 m.

Far sump

This survey was done to verify the location of an old sewage sump and to estimate its lateral extent. The expected location from station drawings is at point N and is labeled far sump in Figure 5, where three parallel survey lines are located. The lines were 100 m long and spaced 15 m apart. In January 1991, using hot point drills provided by CRREL, M&E personnel determined that the depth to contamination was approximately 12 m. The lateral radius of this contaminated zone was estimated to be about 21 m. This sump has not been in use for many years and has refrozen.

We used the 400-MHz transducer unit at a time range of 200 ns to show approximately 20 m of signal penetration into the firn. The three 100-m long parallel time section profiles (lines HI, JK and LM) are shown in Figure 15. The profiles are 15 m apart. Only the center line, JK, shows diffractions in the area of the sewage sump at 50 to 55 m distance. An early hyperbola at 2.4 m depth is from air waves reflecting off a surface object because its slope gives a refractive index less than 1.1. A series of hyperbolas originate at a depth of about 6.5 m and extend vertically down through the record. Their slopes give a refractive index of 1.39 ($\varepsilon = 1.93$). The dip in the layering horizons on either side of the sump are similar to those seen around sump 2 in Figure 13 and is further evidence for firn subsidence around the sumps. None of the diffractions originating near 12 m depth are of unusual intensity, but at the 16- to 17-m depth, the diffractions become more in-

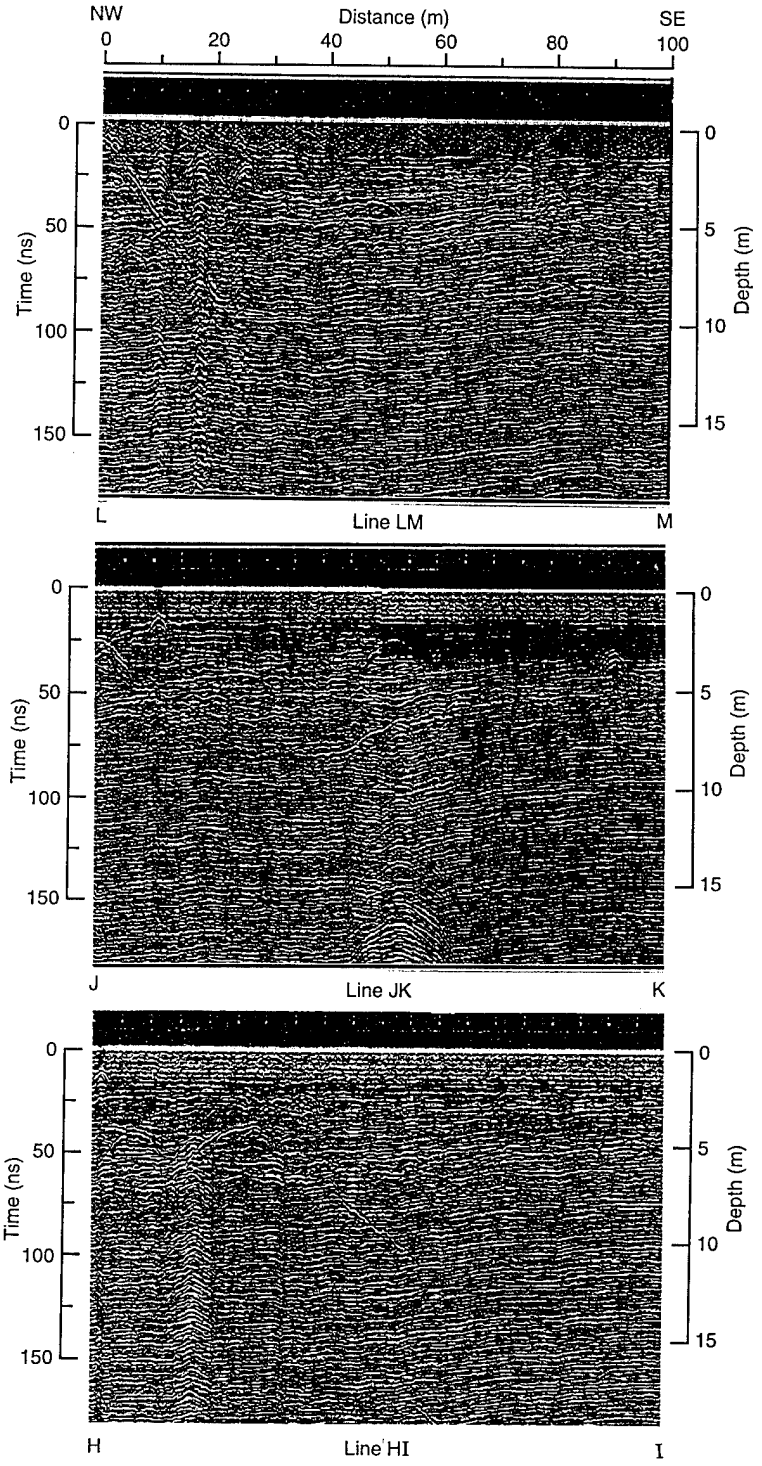

Figure 15. Three parallel 400-MHz profiles recorded at 200 ns at the far sump location (lines HI, JK, LM in Figure 5). Only line JK picked up diffractions at depth.

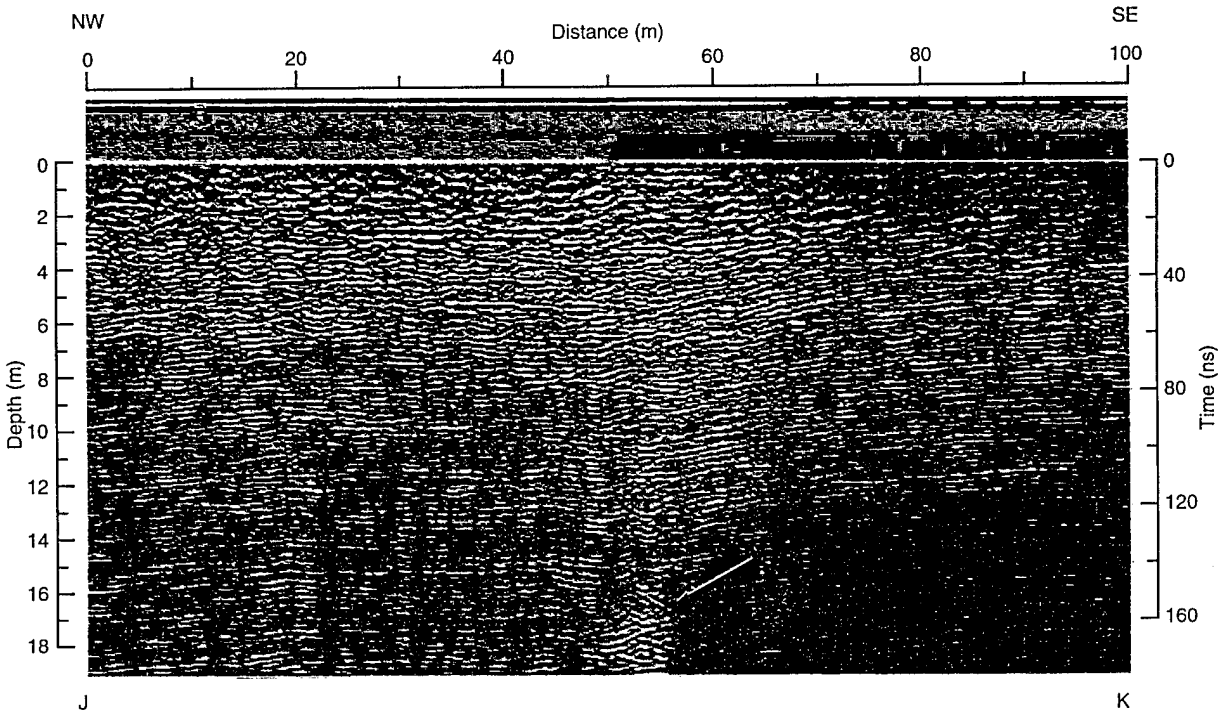

Figure 16. Migration of the profile along the centerline JK at the far sump. A concentration of sewage beginning at about 14 m depth is apparent, but there is no indication of the lateral spreading reported to exist.

tense. The migration of this record (Fig. 16) picks up these deeper targets, which probably represent layers of contaminated snow deeper in the sump. The radar records again suggest less lateral spread of contamination from the discharge point than the 21 m estimated by M&E.

An additional profile, 133 m long, was run from the center of the far sump back to the lift station (line NO in Fig. 5) to determine if any cavities had been created by leaks along the sewer line that serviced the far sump. Some years ago, a leak along the line servicing sump 2 (see Fig. 5) created a 1-m-diameter vertical shaft that was about 30 m deep. A worker clearing snow from the line almost fell into that shaft, which shortly after became sump 1. Figure 17 shows the time section of line NO. The time range is 400 ns and the depth scale is based on $n_m = 1.60$, derived from the deep diffractions from the sump at point N. This value gives a minimum depth scale because the shallow diffractions from buried objects between 25 and 55 m away from the sump (these are too shallow to be leaks) give $n_m = 1.30$. The profile has been horizontally filtered to remove most of the response to the firn layering and is presented in a signal intensity format so that diffractions can be viewed more easily. As in profile JK of Figure 15, there are strong diffractions beginning at the center of the sewage sump (point N) at about 15 to 30 m depth. Strong diffractions, apparently from the utilidor, also occur at point O. Migration of this profile shows no sewage spread beyond about 10-m radius at point N, considerably less than the 21 m estimated by M&E.

Several diffractions occur between the sump and utilidor that could be leaks along the sewer line. Although not easily visible in Figure 17, a cluster of weak diffractions between 64 and 80 m are candidates for shafts caused by leaks. The diffraction at 30 m depth about 93 m from N may be frozen sewage at the base of such a shaft.

Proposed tunnel routes

ASTRO to main station

The two tunnel routes studied are shown in Figure 18. The upper route is divided into sections lettered A, B and C. So much buried debris was detected within the section A survey (originally 30 m wide) just west of the skiway that the width of that section was increased by 10 m to the south and 20 m to the north. Section D in Figure 18 is a narrow swath surveyed between the ASTRO facility and the elevated dormitory. All surveys consisted of parallel profiles, about 2.8 m apart, running the length of the sections. The profiles are alphabetically lettered and may be located later in Figures 21 and 22.

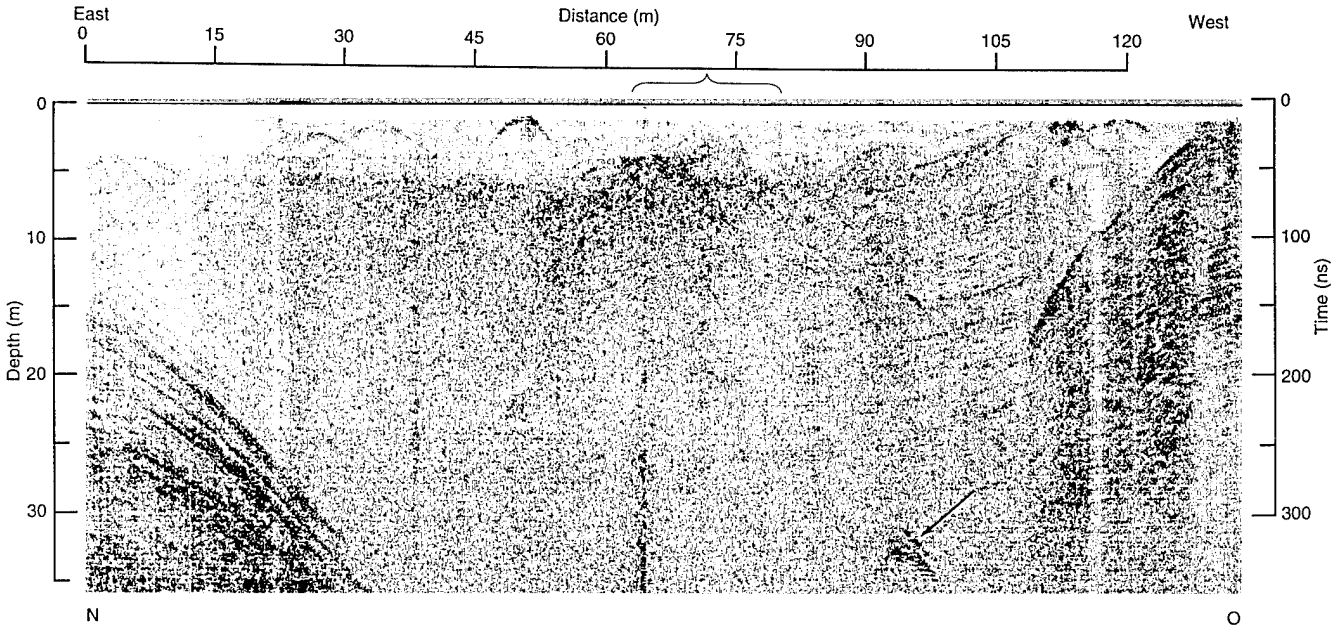

Figure 17. 400-MHz time-section profile from the center of the far sump (point N) back toward the lift station. The diffractions beginning at about 15 m depth at point N are responses to the frozen sewage, but there is no indication of the lateral spreading previously reported because all these diffractions originate near point N. The bracket spans a cluster of weak diffractions whose depth indicates that they may be an old sewer leak, and the arrow points to a deep anomaly of unknown origin.

The profiles of lines D and G within section A are shown in Figure 19. The accuracy of the distance scale depended on accurate electronic marker recording at the moment of passing the flagged stations. This became progressively more difficult as the lines moved farther from the flags and so distance accuracy is probably ±2 m at best. The depth scale is calculated from the value of $n_m = 1.4$, which is the maximum found from diffractions within the firn. Therefore, this value gives the minimum possible depth to the objects (apexes of the diffractions). The profiles are presented in a signal intensity format that emphasizes only the stronger events. Both profiles show a heavy concentration of diffractions just west of the skiway. This concentration is characteristic of most profiles in this section and is the most formidable obstacle in the tunnel survey. Further to the west

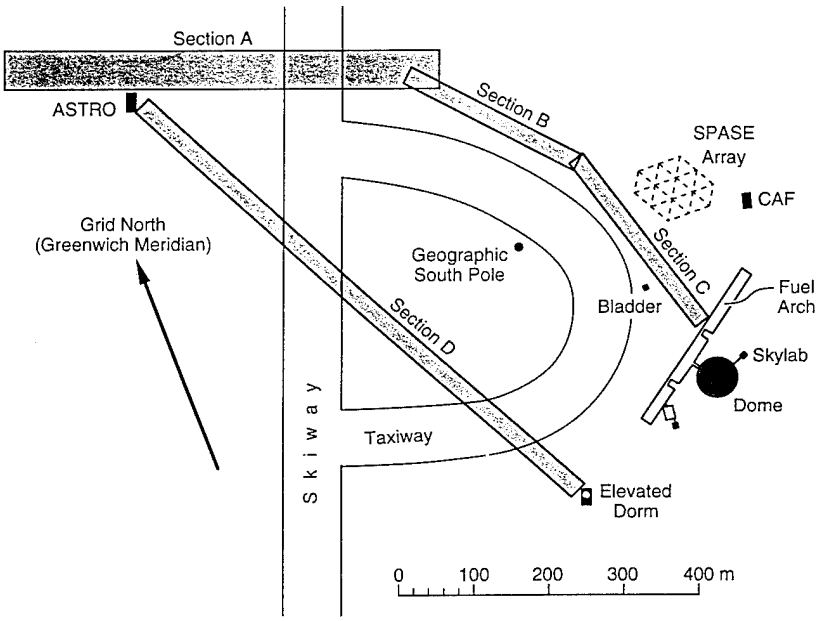

Figure 18. Proposed tunnel routes. Sections A, B and C run from the dome to the ASTRO and CARA (under construction) astronomical facilities. Section D is a 10-m wide section that extended 800 m from the ASTRO building to the elevated dormitory across the skiway.

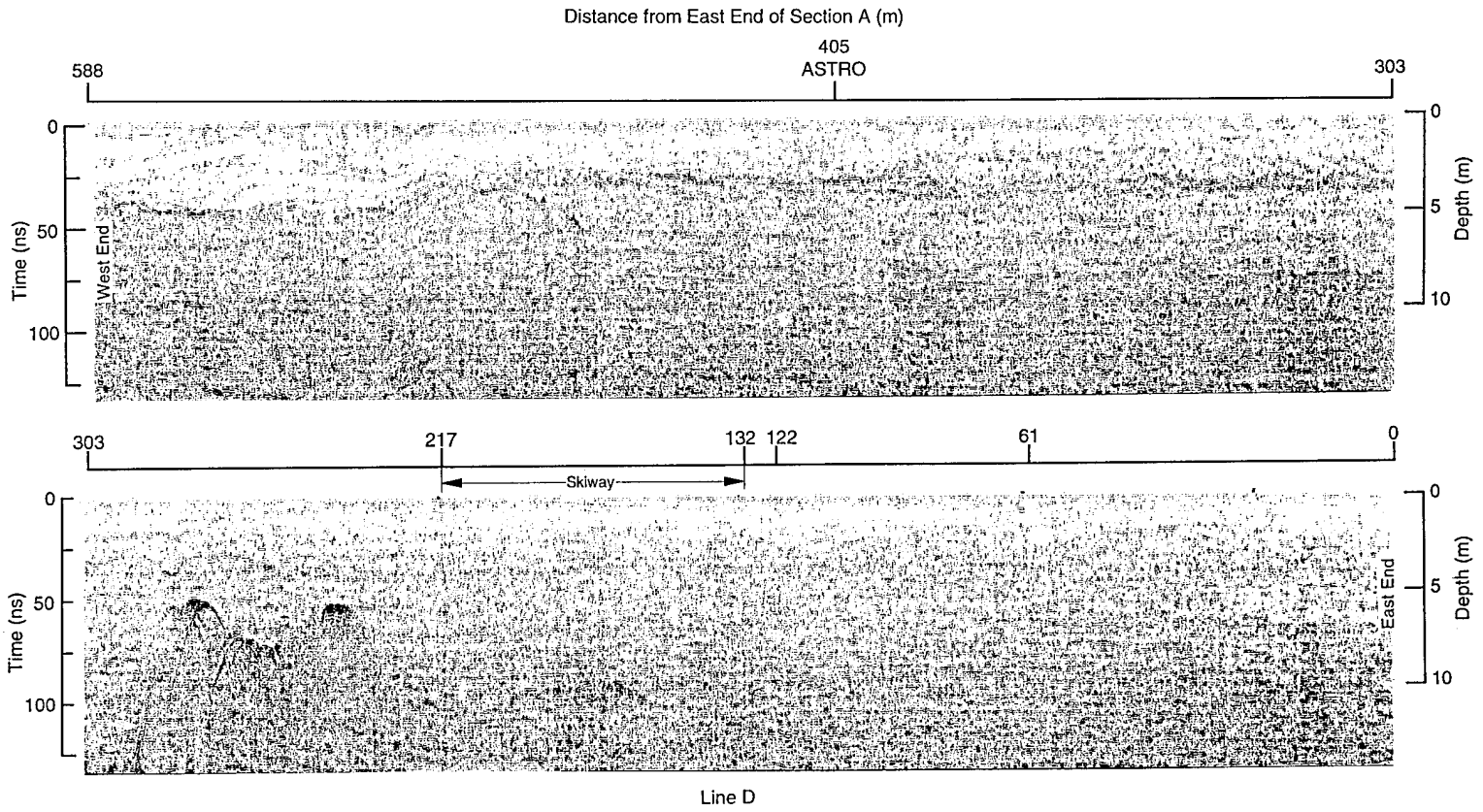

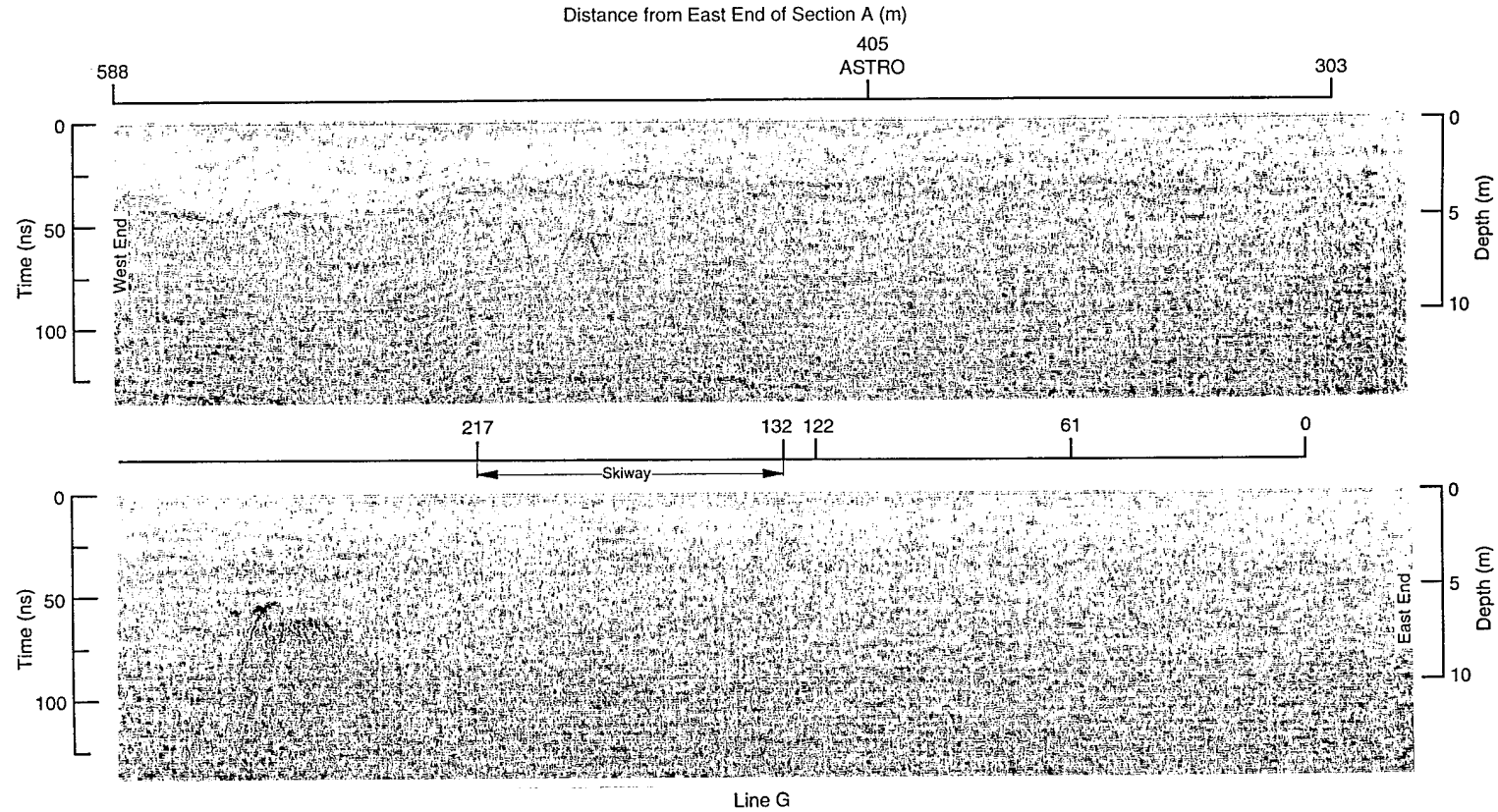

Figure 19. Profiles of lines D and G along section A of the tunnel survey. The depth scale is based on ε = 1.93. Many hyperbolic diffractions can be seen just west of the skiway. A horizon at 4- to 5-m depth is the work surface from previous operations at the first pole station established in 1957.

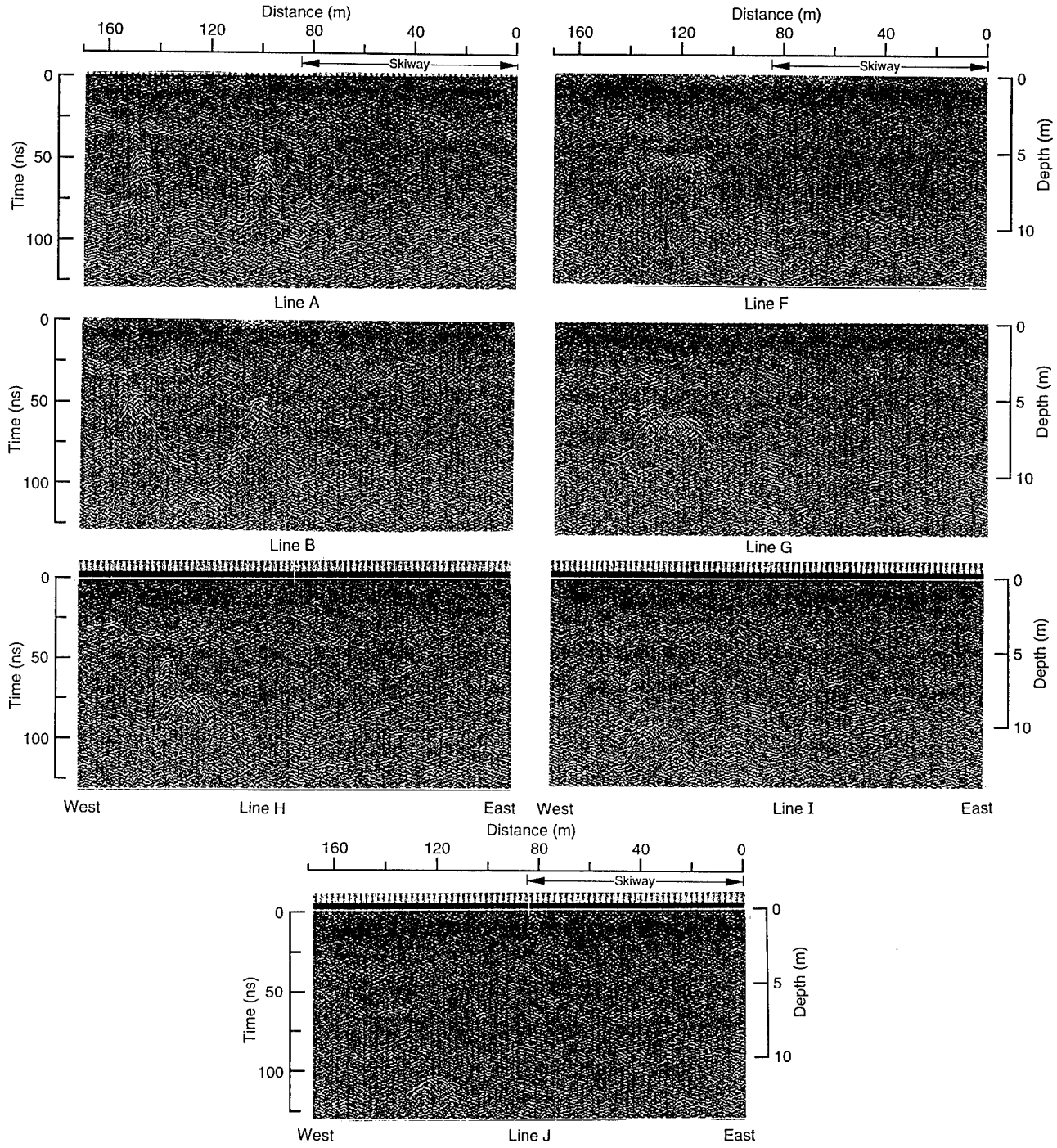

Figure 20. Segments of lines CC–J that contain the many diffractions west of the skiway. The apexes of the diffractions rise as the transects progress to the north (toward line J).

beyond the ASTRO complex several solitary diffractions may be seen. The location and depth of all these diffractions are plotted later in Figure 21. Also visible in Figure 19 is a horizon at about 3 to 4 m depth. This is believed to be dense snow caused by traffic between the old and new stations during the early 1970's when the new station was being constructed.

All radar profiles from line CC (southernmost line) to line J contained diffractions, with most concentrated in the 85-m-wide strip just west of the skiway. No diffractions were seen along lines K through Q in this 85-m-wide area. These 85-m-long profile segments along with the skiway itself are shown in Figure 20. Lines CC through A show responses from distinct targets. The re-

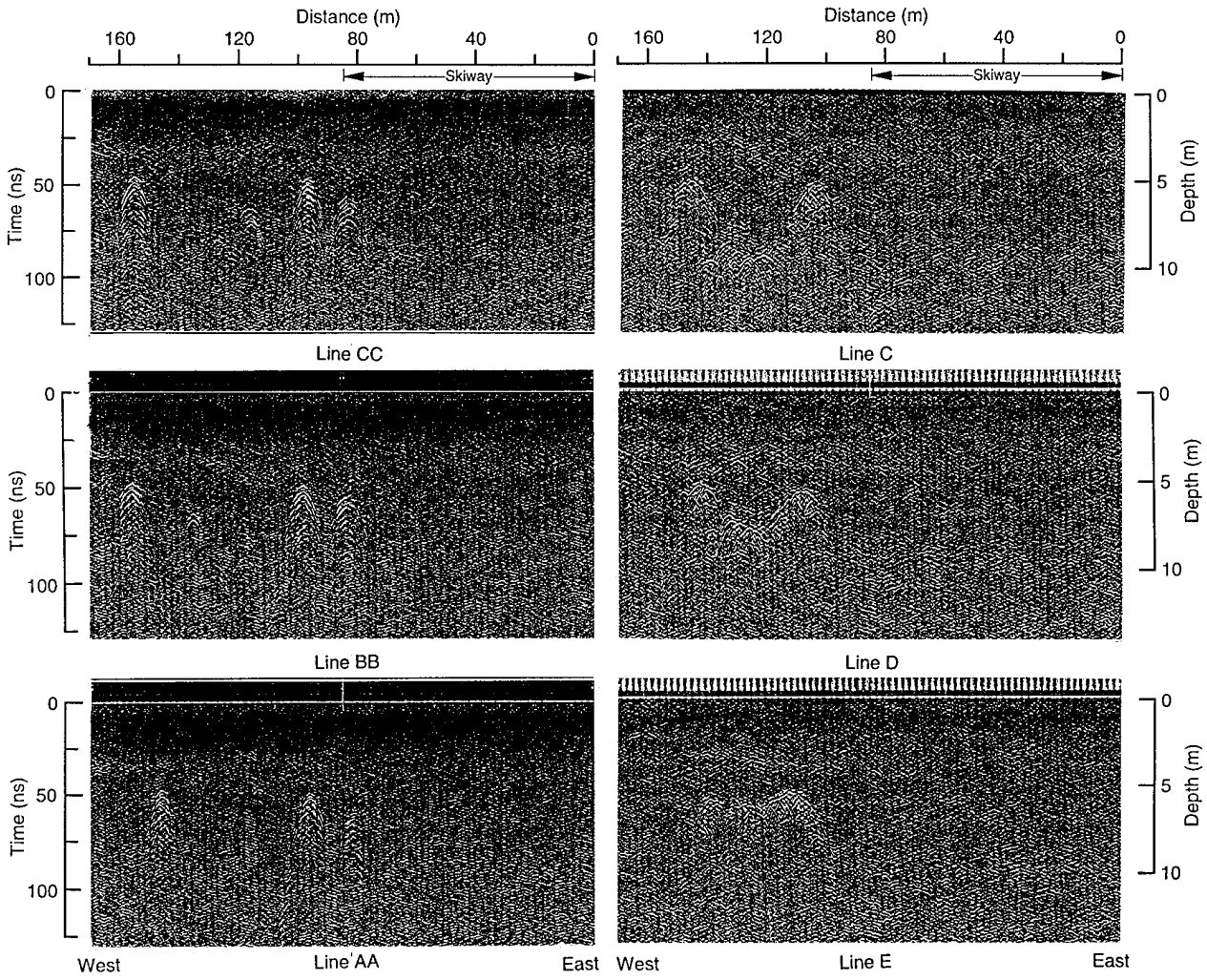

Figure 20 (cont'd).

maining lines A through J each show a continuum of diffractions that represent a considerable amount of debris ranging in depth from 6–12 m. As shown in Figure 21, this debris resides in a line. Perhaps it is an old trash dump.

The skiway, all of section A east of the skiway, all of section B and almost half of section C are clear. There are many indications of debris along the tunnel route west of the ASTRO facility, and also along the easterly half of section C in the vicinity of the fuel bladder by the taxiway. Some of the dots in Figure 21 form linear patterns that may indicate utility lines or orderly storage of abandoned equipment.

Most of the debris near the fuel bladder is located at a depth of less than 4.3 m. Since the top of the tunnel will be at least 4.6 m below the surface, most of the debris in this area should not be a problem, and a tunnel route can be selected to miss the few deep objects in this area. Alternatively, most of these objects could be dug up since they are not deep.

The debris field just west of the skiway must be avoided. That is possible by routing the tunnel just north of this area where lines K through Q showed no debris.

Scattered debris west of the ASTRO building is located at depths that will cause it to interfere with tunneling. However, safe routes through this area are possible. Our route surveys enabled us to find debris and assess the suitability of tunneling routes, but that work was not conducted to pinpoint the location of each potential problem. An additional radar survey for that purpose will be needed just prior to tunneling.

ASTRO to elevated dormitory

This survey route (section D in Fig. 18) was added to determine the feasibility of tunneling along this route, since new station facilities prob-

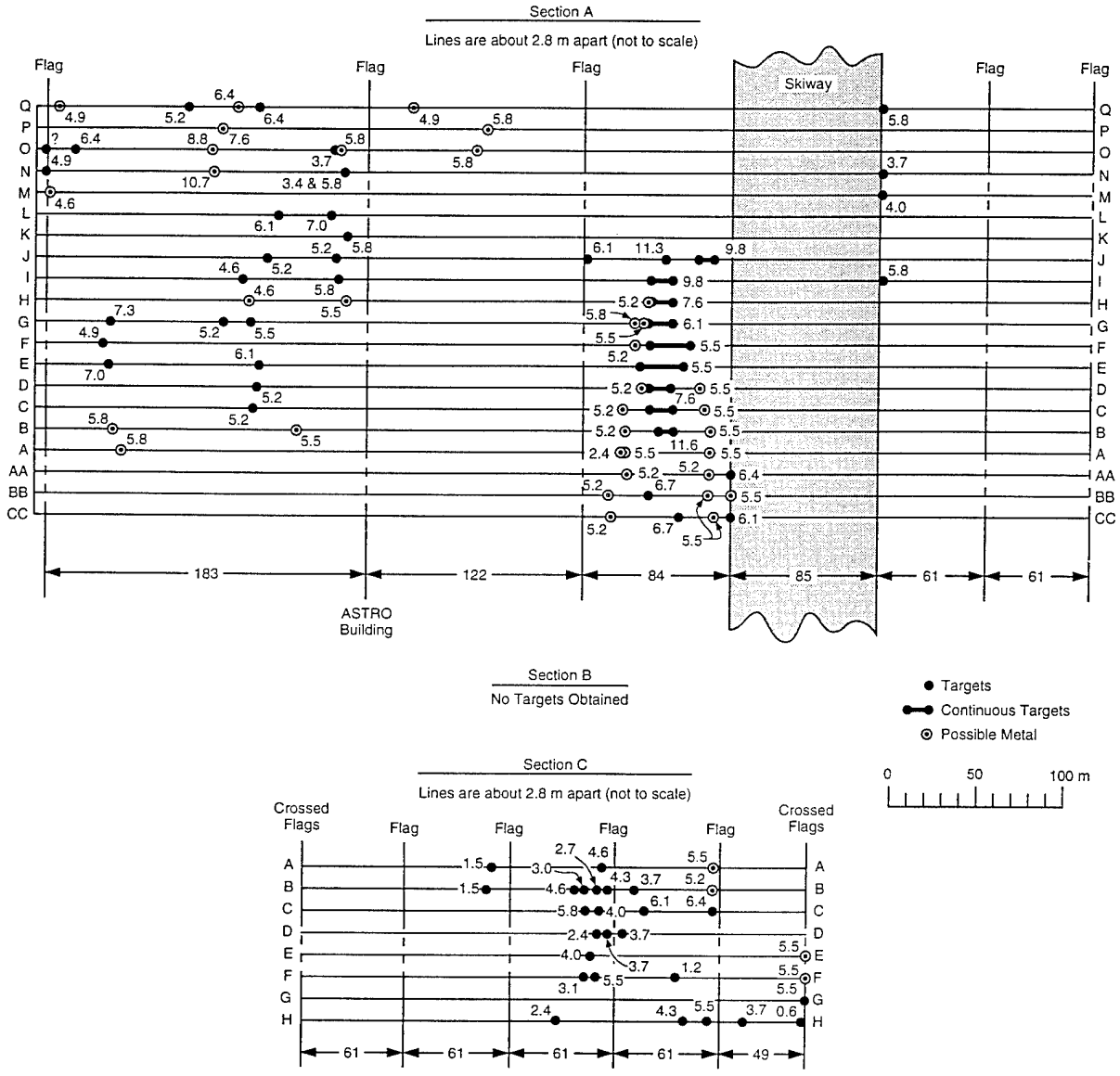

Figure 21. Plan view of the primary tunnel survey. Dots represent radar targets and circled dots are the more intense echoes that are probably from metal targets. Faint reflections may also be metallic targets but with a very small radar cross section. Bars (west of the runway) represent a dense continuum of targets. Numbers beside the dots and bars are depths to the targets in meters. Average line spacing is 2.8 m (not drawn to scale for clarity).

ably will be constructed in this area. The straight route is approximately 800 m long and crosses the skiway and the taxiway. Four lines were run at an average spacing of 2.8 m. The 0-m mark is within a few meters of the ASTRO building.

The results of this survey are shown in Figure 22, where dots mark the approximate location of a diffraction response. Almost the entire route is clear. The accuracy of line and anomaly placement is probably no better than ±5 m because the lines had no intermediate survey marks.

CONCLUSIONS

Radar responses were recorded from numerous subsurface features of interest at the South Pole. Reflections from features of known depth and lateral extent helped calibrate findings. The new water well gave a strong response and its calculated depth was very close to its measured depth. The old clean air facility was located. To mark the spot, a 4-m bamboo pole was placed at point Y in Figure 5. Near its top, a plywood dia-

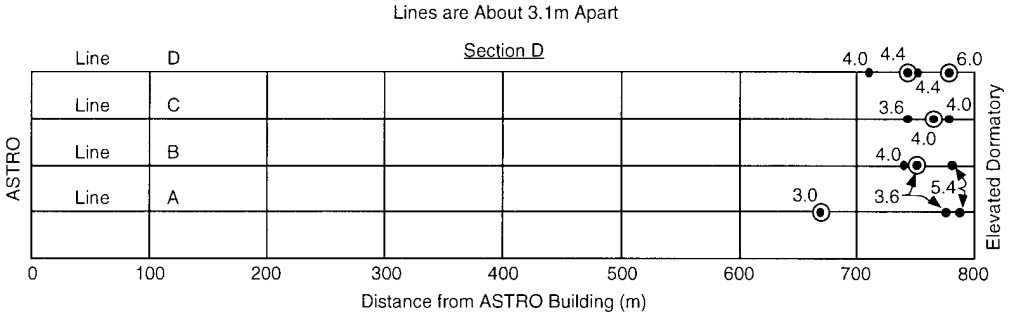

Figure 22. Plan view of the survey run between the ASTRO building and the elevated dormitory. Survey lines begin at the edge of the ASTRO building and terminate at approximately 800 m, about 10 m short of the base of the dormitory. Average survey line spacing is in meters. Dots indicate radar targets with depths in meters indicated.

mond with a Y carved into it is wired to the bamboo. The pole was placed with 2.89 m of its length above the snow surface.

Active and refrozen sewage sumps south of the dome were found, but the radar did not detect their full lateral extent as found in the past by other methods. These sewage sumps are well isolated from the water well. Poor detection of their extent is probably attributable to the low reflectivity of frozen sewage, loss of signal strength at depth, and loss of imaging ability because of the data compression needed to accommodate the migration algorithm. Improved imaging of subsurface structures near the dome would require software that accommodates at least twice as many scans (127) for the migration aperture. Successful imaging of unfrozen sewage at depth in firn at McMurdo station is discussed in Arcone et al. (1994).

Debris just west of the skiway along the tunnel route initially proposed between ASTRO and the main station appears to be large and extensive. The tunnel should be routed just north of this area. A few objects exist in the snow along this new route, but a tunnel route can be found among them with the help of radar.

The GPR was sensitive to many subsurface changes in material properties, including contrasts in firn density caused by traffic. Distorted snow layers around sewage sumps were clearly visible. We did not experience any radio interference, but the radar clutter of surface and near-surface targets would have precluded interpretation of some records had we not had advance knowledge of the approximate location and depth of features of interest. Future investigations to a depth of about 30 m should use a 400- to 600-MHz transducer. Higher frequencies for greater resolution are available, but their depth of penetration may be limited to less than about 20 m by their lower power. Operation of the tape recorder and control unit outside the tracked vehicle was limited by the cold weather, which shortened the usable battery life from 3.5 to about 2 hours.

LITERATURE CITED

Annan, A.P., W.M. Waller, D.W. Strangway, J.R. Rossiter, J.D. Redman and R.D. Watts (1975) The electromagnetic response of a low-loss, 2-layer, dielectric earth for horizontal electric dipole excitation. *Geophysics*, **40**(2): 285–298.

Annan, A.P. and J.L. Davis (1976) Impulse radar profiling in permafrost. *Radio Science*, **11**(4): 383–394.

Arcone, S.A. (1991) Dielectric constant and layer-thickness interpretation of helicopter-borne short-pulse radar waveforms reflected from wet and dry river-ice sheets. *IEEE Transactions on Geoscience and Remote Sensing*, **29**(5): 768–777.

Arcone, S.A. (1995) Numerical studies of the radiation patterns of resistively loaded dipoles. *Journal of Applied Geophysics*, **33**: 39–52.

Arcone, S.A. and A.J. Delaney (1987) Helicopter-borne short-pulse radar profiles of river-ice sheets in Alaska. *Journal of Glaciology*, **97**(1): 333–341.

Arcone, S.A., E.F. Chacho, Jr. and A.J. Delaney (1992) GPR detection of unfrozen water in the Sagavanirktok flood plain, Alaska. *Water Resources Research*, **28**(11): 2925–2936.

Arcone, S.A., A.J. Delaney and W. Tobiasson (1994) Subsurface radar investigations at the Pegasus ice runway and Williams Field, McMurdo Station, Antarctica. USA Cold Regions Research and Engineering Laboratory, CRREL Report 94-12.

Arcone, S.A., D.E. Lawson and A.J. Delaney (1995) Short pulse radar wavelet recovery and resolution of dielectric contrasts within englacial and basal

ice of Matanuska Glacier, Alaska. *Journal of Glaciology*, **41**(137): 68–86.

Bogorodsky, V.V., C.R. Bentley and P.E. Gudmandsen (1985) *Radioglaciology*. Boston, Massachusetts: D. Reidel Publishing Company.

Cumming, W.A. (1952) The dielectric properties of ice and snow at 3.2 centimeters. *Journal of Applied Physics*, **23**(7): 768–773.

Delaney, A.J., S.A. Arcone and E.F. Chacho, Jr. (1991) Winter short-pulse radar studies on the Tanana River, Alaska. *Arctic*, **43**: 244–250.

Engheta, N., C.H. Pappas and C. Elachi (1982) Radiation patterns of interfacial dipole antennas. *Radio Science*, **17**(6): 1557–1566.

Galinovsky, L. and K. Levin (1990) RADAN 3.0 (signal processing software). North Salem, New Hampshire: Geophysical Survey Systems, Inc.

Hanninen, P. and S. Autio (Ed.) (1992) *Proceedings, IV International Conference on Ground Penetrating Radar, 8–13 June 1992, Rovaniemi, Finland.* Espoo, Finland: Geological Survey of Finland, Special Paper 16.

Kovacs, A. and A.J. Gow (1975) Brine infiltration in the McMurdo Ice Shelf, McMurdo Sound, Antarctica. *Journal of Geophysical Research*, **80**(15): 1957–1961.

Kovacs, A. and R.M. Morey (1979) Remote detection of massive ice in permafrost along the Alyeska Pipeline and the pump station feeder gas pipeline. In *Proceedings of the Specialty Conference on Pipelines in Adverse Environments, ASCE, New Orleans, Louisiana*, p. 268–279.

Kovacs, A., A.J. Gow, J.H. Cragin and R.M. Morey (1982) The brine zone in the McMurdo Ice Shelf, Antarctica. USA Cold Regions Research and Engineering Laboratory, CRREL Report 82-39.

Pilon, J. (Ed.) (1992) *Proceedings, II International Conference on Ground Penetrating Radar, Ottawa, Canada, 26–28 May 1988*. Ottawa: Canadian Research Council, Department of Energy, Mines and Resources. Geological Survey of Canada Paper 90-4.

Yilmaz, O. (1987) *Seismic Data Processing*. Tulsa, Oklahoma: Society of Exploration Geophysicists.

REPORT DOCUMENTATION PAGE

Form Approved
OMB No. 0704-0188

1. AGENCY USE ONLY (Leave blank)	2. REPORT DATE	3. REPORT TYPE AND DATES COVERED
	December 1995	

4. TITLE AND SUBTITLE
Ground-Penetrating Radar Investigation of the Proposed Dome–CARA Tunnel Route, and Utilities at South Pole Station, Antarctica

5. FUNDING NUMBERS
DPP-872 0063

6. AUTHORS
Steven A. Arcone, Wayne Tobiasson and Allan J. Delaney

7. PERFORMING ORGANIZATION NAME(S) AND ADDRESS(ES)
U.S. Army Cold Regions Research and Engineering Laboratory
72 Lyme Road
Hanover, New Hampshire 03755-1290

8. PERFORMING ORGANIZATION REPORT NUMBER
CRREL Report 95-24

9. SPONSORING/MONITORING AGENCY NAME(S) AND ADDRESS(ES)
National Science Foundation
Arlington, Virginia 22230

10. SPONSORING/MONITORING AGENCY REPORT NUMBER

11. SUPPLEMENTARY NOTES

12a. DISTRIBUTION/AVAILABILITY STATEMENT
Approved for public release; distribution is unlimited.

Available from NTIS, Springfield, Virginia 22161.

12b. DISTRIBUTION CODE

13. ABSTRACT (*Maximum 200 words*)

Ground-penetrating radar studies were performed at South Pole Station, Antarctica, during January 1993 to determine if subsurface obstructions exist along a planned tunnel route from the main station to the new astrophysical research area on the far side of the skiway, and if various man-made subsurface features such as sewage sumps, a water well, utilidors and buried buildings could be located and delineated. The maximum depth of interest for the tunnel survey was approximately 10 m. For it, a short-pulse antenna transducer with its antenna bandwidth centered near 400 MHz was towed along the ground surface over multiple traverses to cover an area up to 60 m wide. The survey extended from the South Pole Station fuel arch, across the skiway and then to the CARA site (Center for Astrophysical Resarch in Antarctica). The radar profiles show reflections from density layering within the snow caused by traffic and diffractions from artificial features within 13 m depth. Debris is present in the snow west of the skiway and near the fuel bladder near the taxiway. Targets within 100 m of the west side of the skiway are extensive, and appear to be metallic. The tunnel should be routed in the clear area north of them. Targets near the fuel bladder are only 3 to 4 m below the surface. The tunnel could go under them, but as a precaution they could be removed. An additional survey was run over a 30-m-wide swath from the ASTRO facility at the CARA site to the new elevated dormitory, a distance of approxi-

14. SUBJECT TERMS		15. NUMBER OF PAGES
Antarctica	Ground-penetrating radar	32
Cold regions	South Pole Station	16. PRICE CODE
GPR	Tunnel survey	

17. SECURITY CLASSIFICATION OF REPORT	18. SECURITY CLASSIFICATION OF THIS PAGE	19. SECURITY CLASSIFICATION OF ABSTRACT	20. LIMITATION OF ABSTRACT
UNCLASSIFIED	UNCLASSIFIED	UNCLASSIFIED	UL

13. ABSTRACT (CONT'D)

mately 800 m. This swath appears to be clear of any subsurface debris, except very near the dormitory. Surveys performed at several utility sites near the main station provided a general assessment of the dielectric properties of the firn, and tested the radar's ability to delineate subsurface features and potential hazards. Migrated, spatial images of the old clean air facility, the water well under development, and the several sewage sumps are presented. In general, the numerous vents, cables, antennas, etc., of the area clutter the profiles with diffractions that complicate interpretation of the data without prior knowledge of some features. The migrated images allowed approximations to be made as to the depths of sewage sumps, the water well and the old buried clean air facility.